Chapter 5

Resistance and Mobility Relations

5.1 Introduction

In this chapter, we address a specific issue, the linear relation between the moments of the surface tractions on a rigid particle and the parameters that govern the relative motion of the particle through a flowing viscous fluid, and follow that with examples to illustrate the use of these relations in suspension theory. As before, we assume that the length scale for the macroscopic problem and that for the microstructure (particle size) are well separated. So on an intermediate length scale that is still much greater than the particle size, we may take the ambient fluid flow field as a combination of a uniform streaming velocity plus a linear field (constant velocity gradient). In other words, the particle interacts with a fluid environment described by the ambient flow field, $\boldsymbol{U}^\infty + \boldsymbol{\Omega}^\infty \times \boldsymbol{x} + \boldsymbol{E}^\infty \cdot \boldsymbol{x}$, with the usual decomposition of the linear term into rotational and rate-of-strain fields. Steady external forces and torques acting on the particles (*e.g.*, gravity, electromagnetic fields) will produce a rigid-body motion of the particle, $\boldsymbol{U} + \omega \times \boldsymbol{x}$, of just the right proportion to balance the resulting hydrodynamic forces and torques with these external agents, as required by Newton's law.

In the next four sections of this chapter we focus our attention on three quantities (the hydrodynamic force $\boldsymbol{F}$, torque $\boldsymbol{T}$, and stresslet $\boldsymbol{S}$ exerted by the fluid on the particle). These are followed by two sections on applications. We examine the theory for the rheological behavior of a dilute suspension of nonspherical particles and show how the resistance functions are used in the development of the theory. In Section 5.7, we discuss *electrophoresis*, or the motion of a charged particle through a viscous electrolyte under the influence of an applied electric field. The role of the resistance functions in the balance between hydrodynamic and electrical forces is examined. A derivation of the electrophoretic mobility for the important limiting cases of thin (Smoluchowski limit) and thick (Hückel limit) are included. We show how the Lorentz reciprocal theorem gives directly the famous result of Smoluchowski that the

electrophoretic mobility is independent of the particle geometry in the limit of thin double layers.

From these two applications, it will become clear that microhydrodynamic calculations alone do not provide a complete description of the physics. For example, the rheological behavior of a suspension is also dependent on the orientation distribution function and Brownian motion plays an important role therein, while the analysis of electrophoretic motion requires an additional set of physical laws to describe the effect of the ion (charge) distribution. However, these examples illustrate the ways in which the resistance and mobility function play an integral role in the mathematical analysis; for as long as viscous forces are important, microhydrodynamics will be called upon to convert information concerning forces acting on a particle into a prescription for particle motion.

5.2 The Resistance Tensor

The setting for this and three subsequent sections is a particle undergoing rigid-body motion in a linear ambient field. We focus our attention on three quantities — the hydrodynamic force $\boldsymbol{F}$, torque $\boldsymbol{T}$ and stresslet $\boldsymbol{S}$ — exerted by the fluid on the particle. From the viewpoint of a mathematical boundary value problem, it is quite natural to set the particle and fluid velocities (the boundary conditions) and then calculate $\boldsymbol{F}$, $\boldsymbol{T}$ and $\boldsymbol{S}$. This so-called resistance problem is the subject of this section, and the discussion follows closely the exposition of Brenner [10]. In *mobility* problems, $\boldsymbol{F}$ and $\boldsymbol{T}$ are given and the relative motion of the particle through the fluid is to be determined. These problems are discussed in Section 5.3 and the connection between the two are given in Section 5.4.

In the problem at hand, the disturbance velocity field has the boundary condition at the particle surface

$$\boldsymbol{v}^D(\boldsymbol{x}) = \boldsymbol{U} - \boldsymbol{U}^\infty + (\boldsymbol{\omega} - \boldsymbol{\Omega}^\infty) \times \boldsymbol{x} - \boldsymbol{E}^\infty \cdot \boldsymbol{x} \,, \qquad \boldsymbol{x} \in S \,.$$

Since the governing equations are linear, we may decompose the resistance problem into three simpler problems:

1. Translation of the particle with a steady velocity $\boldsymbol{U} - \boldsymbol{U}^\infty$ through a quiescent fluid.

2. Rotation of the particle with a steady angular motion, $(\boldsymbol{\omega} - \boldsymbol{\Omega}^\infty) \times \boldsymbol{x}$, in a quiescent fluid. We defer until Section 5.2.2 a discussion on the choice of the center of rotation.

3. A fixed particle in a rate-of-strain field $\boldsymbol{E}^\infty \cdot \boldsymbol{x}$.

For the first problem, we may again exploit linearity plus dimensional analysis to assert that the relation between the $\boldsymbol{F}$ and $\boldsymbol{U} - \boldsymbol{U}^\infty$ must be of the form

$$\boldsymbol{F} = \mu \boldsymbol{A} \cdot (\boldsymbol{U}^\infty - \boldsymbol{U}) \,,$$

where $\boldsymbol{A}$ is a second order-tensor with dimension of length that depends only on the shape of the particle. While the derivation along these lines is straightforward, Brenner [10] gives the following more elegant proof based on the Lorentz reciprocal theorem. Consider two separate fluid motions produced by translational velocities $\boldsymbol{U}'$ and $\boldsymbol{U}''$. Denote the resulting forces by $\boldsymbol{F}'$ and $\boldsymbol{F}''$. Then from the reciprocal theorem (Chapter 2) we have

$$\boldsymbol{U}' \cdot \boldsymbol{F}'' = \boldsymbol{U}'' \cdot \boldsymbol{F}' \ .$$

We write the relation between the force and translational velocity as $\boldsymbol{F} = \boldsymbol{f}(\boldsymbol{U})$, and replace $\boldsymbol{U}'' \rightarrow \boldsymbol{U}_1 + \boldsymbol{U}_2$ and $\boldsymbol{U}' \rightarrow \boldsymbol{U}_1$. We do this again, only now using $\boldsymbol{U}' \rightarrow \boldsymbol{U}_2$. The resulting equations are

$$\begin{aligned} (\boldsymbol{U}_1 + \boldsymbol{U}_2) \cdot \boldsymbol{f}(\boldsymbol{U}_1) &= \boldsymbol{U}_1 \cdot \boldsymbol{f}(\boldsymbol{U}_1 + \boldsymbol{U}_2) \\ (\boldsymbol{U}_1 + \boldsymbol{U}_2) \cdot \boldsymbol{f}(\boldsymbol{U}_2) &= \boldsymbol{U}_2 \cdot \boldsymbol{f}(\boldsymbol{U}_1 + \boldsymbol{U}_2) \ , \end{aligned}$$

and by combining the two, we find the relation,

$$(\boldsymbol{U}_1 + \boldsymbol{U}_2) \cdot (\boldsymbol{f}(\boldsymbol{U}_1 + \boldsymbol{U}_2) - \boldsymbol{f}(\boldsymbol{U}_1) - \boldsymbol{f}(\boldsymbol{U}_2)) = 0 \ .$$

Since $\boldsymbol{U}_1$ and $\boldsymbol{U}_2$ are arbitrary, we conclude that $\boldsymbol{f}(\boldsymbol{U}_1 + \boldsymbol{U}_2) = \boldsymbol{f}(\boldsymbol{U}_1) + \boldsymbol{f}(\boldsymbol{U}_2)$, *i.e.*, the relation is linear.[1]

Generalizing these ideas, the linearity of the Stokes equations leads to the set of linear relations between the moments and the flow parameters [15]:

$$\begin{pmatrix} \boldsymbol{F} \\ \boldsymbol{T} \\ \boldsymbol{S} \end{pmatrix} = \mu \begin{pmatrix} \boldsymbol{A} & \tilde{\boldsymbol{B}} & \tilde{\boldsymbol{G}} \\ \boldsymbol{B} & \boldsymbol{C} & \tilde{\boldsymbol{H}} \\ \boldsymbol{G} & \boldsymbol{H} & \boldsymbol{M} \end{pmatrix} \begin{pmatrix} \boldsymbol{U}^\infty - \boldsymbol{U} \\ \boldsymbol{\Omega}^\infty - \boldsymbol{\omega} \\ \boldsymbol{E}^\infty \end{pmatrix} \ . \tag{5.1}$$

The square matrix is the *resistance matrix*, sometimes called the grand resistance matrix to distinguish from the subcases (sub-block matrices); it contains second-rank tensors $\boldsymbol{A}$, $\boldsymbol{B}$, and $\boldsymbol{C}$, third-rank tensors $\boldsymbol{G}$ and $\boldsymbol{H}$, and a fourth-rank tensor $\boldsymbol{M}$. The fluid viscosity has been scaled from these quantities so that the matrix elements have dimensions of length to the first ($\boldsymbol{A}$), second ($\boldsymbol{B}$, $\boldsymbol{G}$), or third ($\boldsymbol{C}$, $\boldsymbol{H}$, and $\boldsymbol{M}$) powers. The multiplication rules for the matrix elements in the above equation are the tensorial inner products, as in

$$\begin{aligned} F_i &= \mu A_{ij}(U_j^\infty - U_j) + \mu \tilde{B}_{ij}(\Omega_j^\infty - \omega_j) + \mu \tilde{G}_{ijk} E_{jk}^\infty \ , \\ S_{ij} &= \mu G_{ijk}(U_k^\infty - U_k) + \mu H_{ijk}(\Omega_k^\infty - \omega_k) + \mu M_{ijkl} E_{kl}^\infty \ . \end{aligned}$$

Tildes are employed for the upper triangular elements of the resistance matrix because the tensors are not independent, as we now show.

[1]Strictly speaking, this only shows that projections onto the sum vector satisfy linearity. To finish the proof, use $f(U) = f(U) \cdot e_i e_i = f(e_i) \cdot U e_i = (e_i f(e_i)) \cdot U$.

5.2.1 Symmetry and Positive Definiteness

We will show that the grand resistance matrix is symmetric, *i.e.*,

$$\begin{aligned} A_{ij} &= A_{ji} \ , \quad & C_{ij} &= C_{ji} \ , \quad & M_{ijkl} &= M_{klij} \ , \\ B_{ij} &= \tilde{B}_{ji} \ , \quad & G_{ijk} &= \tilde{G}_{kij} \ , \quad & H_{ijk} &= \tilde{H}_{kij} \ , \end{aligned}$$

as a consequence of the Lorentz reciprocal theorem. The proofs for the six symmetry relations are similar. We shall prove the relation for $\boldsymbol{A}$ and $\boldsymbol{H}$, and leave the rest for Exercise 5.1.

To show that $\boldsymbol{A}$ is symmetric, start once more from $\boldsymbol{U}' \cdot \boldsymbol{F}'' = \boldsymbol{U}'' \cdot \boldsymbol{F}'$, and let $\boldsymbol{U}'$ and $\boldsymbol{U}''$ correspond to motions in the i-th and j-th coordinate directions. For the $\boldsymbol{H}$ relation, the same idea applies. We start with the following statement of the Lorentz reciprocal theorem:

$$\oint_S \boldsymbol{v}_1 \cdot \boldsymbol{\sigma}_2 \cdot \boldsymbol{n} \, dS = \oint_S \boldsymbol{v}_2 \cdot \boldsymbol{\sigma}_1 \cdot \boldsymbol{n} \, dS \ . \tag{5.2}$$

For the first velocity field, we take the disturbance field of the particle fixed in a straining motion $\boldsymbol{E}^\infty \cdot \boldsymbol{x}$, while for the second we choose the disturbance field generated by the particle rotating with velocity $\boldsymbol{\omega}$ in the ambient field $\boldsymbol{\Omega}^\infty \times \boldsymbol{x}$. These two velocity fields vanish at infinity, while on the particle surface the boundary conditions require

$$\boldsymbol{v}_1(\boldsymbol{x}) = -\boldsymbol{E}^\infty \cdot \boldsymbol{x} \ , \qquad \boldsymbol{v}_2(\boldsymbol{x}) = \boldsymbol{\omega} \times \boldsymbol{x} - \boldsymbol{\Omega}^\infty \times \boldsymbol{x} \ . \tag{5.3}$$

The particle torque and stresslet in these two flows follow from the definitions of the resistance functions as

$$T_k = \oint_{S_p} [\boldsymbol{x} \times (\boldsymbol{\sigma}_2 \cdot \boldsymbol{n})]_k \, dS = \tilde{H}_{kij} E^\infty_{ij} \tag{5.4}$$

and

$$S_{ij} = \frac{1}{2} \oint_{S_p} [x_i (\boldsymbol{\sigma}_1 \cdot \boldsymbol{n})_j + (\boldsymbol{\sigma}_1 \cdot \boldsymbol{n})_i x_j] \, dS = H_{ijk} (\Omega^\infty_k - \omega_k) \ . \tag{5.5}$$

The torque evaluated with the disturbance stress field $\boldsymbol{\sigma}_1$ equals that of the complete solution because the undisturbed straining motion, $\boldsymbol{E}^\infty \cdot \boldsymbol{x}$, does not generate a torque.

For the surface in the reciprocal theorem, we take the boundaries of the fluid region between the particle and a large spherical surface "at infinity." The contributions from the latter vanish because the fields decay far away from the particle at least as fast as $\boldsymbol{v}_1 \sim O(r^{-1})$, $\boldsymbol{v}_2 \sim O(r^{-1})$, $\boldsymbol{\sigma}_1 \sim O(r^{-2})$, $\boldsymbol{\sigma}_2 \sim O(r^{-2})$.[2] The contributions on the particle surface are simplified using the boundary conditions, Equation 5.3.

[2] A straining field about, or rotational motions of, the general particle may contain a monopole field.

Since $\boldsymbol{v}_1$ is the disturbance in the straining field, we have

$$\begin{aligned} -\oint_S (\boldsymbol{v}_1)_i(\boldsymbol{\sigma}_2 \cdot \boldsymbol{n})_i \, dS &= \oint_S E^\infty_{ij} x_j (\boldsymbol{\sigma}_2 \cdot \boldsymbol{n})_i \, dS \\ &= E^\infty_{ij} \oint_S x_j (\boldsymbol{\sigma}_2 \cdot \boldsymbol{n})_i \, dS \\ &= E^\infty_{ij} \frac{1}{2} \oint_S \left(x_i (\boldsymbol{\sigma}_2 \cdot \boldsymbol{n})_j + x_j (\boldsymbol{\sigma}_2 \cdot \boldsymbol{n})_i \right) dS \\ &= E^\infty_{ij} H_{ijk} (\Omega^\infty_k - \omega_k) \, . \end{aligned} \tag{5.6}$$

To go from the second to the third line, we used $E^\infty_{ij} = E^\infty_{ji}$ to symmetrize the force dipole into the stresslet, and the last step invoked Equation 5.5.

Similarly, with $\boldsymbol{v}_2$ as the disturbance field of the rotational problem, we have

$$\begin{aligned} -\oint_S (\boldsymbol{v}_2)_i(\boldsymbol{\sigma}_1 \cdot \boldsymbol{n})_i \, dS &= \oint_S \epsilon_{ikj} (\boldsymbol{\Omega}^\infty_k - \boldsymbol{\omega}_k) x_j (\boldsymbol{\sigma}_1 \cdot \boldsymbol{n})_i \, dS \\ &= (\boldsymbol{\Omega}^\infty_k - \boldsymbol{\omega}_k) \oint_S \epsilon_{kji} x_j (\boldsymbol{\sigma}_1 \cdot \boldsymbol{n})_i \, dS \\ &= (\boldsymbol{\Omega}^\infty_k - \boldsymbol{\omega}_k) \tilde{H}_{kij} E^\infty_{ij} \, . \end{aligned} \tag{5.7}$$

To go from the second to the third line, we used Equation 5.4 for the torque on the particle in a straining field.

Combining Equations 5.6 and 5.7 gives

$$E^\infty_{ij} H_{ijk} (\Omega^\infty_k - \omega_k) = (\boldsymbol{\Omega}^\infty_k - \boldsymbol{\omega}_k) \tilde{H}_{kij} E^\infty_{ij} \, . \tag{5.8}$$

But $\boldsymbol{\Omega}^\infty - \boldsymbol{\omega}$ and $\boldsymbol{E}^\infty$ are arbitrary constants, so we have

$$H_{ijk} = \tilde{H}_{kij} \, , \tag{5.9}$$

as claimed. Having shown that the grand matrix is symmetric, we now show that it is positive-definite.

The rate of energy dissipation (Chapter 2) of the disturbance field is given by

$$\int_V e^D_{ij} e^D_{ij} \, dV = -\oint_{S_p} v^D_i \sigma^D_{ij} \hat{n}_j \, dS \, .$$

The disturbance stress field is given everywhere by $\boldsymbol{\sigma}^D = \boldsymbol{\sigma} - 2\mu \boldsymbol{E}^\infty$, and on the particle surface we have $\boldsymbol{v}^D = \boldsymbol{U} - \boldsymbol{U}^\infty + (\boldsymbol{\omega} - \boldsymbol{\Omega}^\infty) \times \boldsymbol{x} - \boldsymbol{E}^\infty \cdot \boldsymbol{x}$. Inserting these results in above gives the inequality

$$(\boldsymbol{U}^\infty - \boldsymbol{U}) \cdot \boldsymbol{F} + (\boldsymbol{\Omega}^\infty - \boldsymbol{\omega}) \cdot \boldsymbol{T} + \boldsymbol{E}^\infty : \boldsymbol{S} \geq \boldsymbol{E}^\infty : \boldsymbol{S}^\infty = 2\mu V_p \boldsymbol{E}^\infty : \boldsymbol{E}^\infty \, ,$$

where $\boldsymbol{S}^\infty = 2\mu V_p \boldsymbol{E}^\infty$ is the stresslet of the undisturbed rate-of-strain field,

$$\boldsymbol{S}^\infty = 2\mu V_p \boldsymbol{E}^\infty = \frac{1}{2} \oint_{S_p} \left[(\boldsymbol{\sigma}^\infty \cdot \hat{\boldsymbol{n}}) \boldsymbol{x} + \boldsymbol{x} (\boldsymbol{\sigma}^\infty \cdot \hat{\boldsymbol{n}}) \right] dS \, .$$

We replace $\boldsymbol{F}$, $\boldsymbol{T}$, and $\boldsymbol{S}$ using the resistance relation, and the resulting inequality establishes that the grand resistance matrix is positive-definite. We may take

special cases, *e.g.*, translational motion alone, or just rotational motion, or pure straining motion about a fixed particle, to show that the diagonal elements $\boldsymbol{A}$, $\boldsymbol{C}$, and $\boldsymbol{M}$ are positive-definite tensors.

Now that we know that $\boldsymbol{A}$ is a symmetric, positive-definite, second order tensor, we arrive at the following conclusions:

1. There are three mutually orthogonal axes, given by the principal directions of $\boldsymbol{A}$. Translations through a quiescent fluid along one of these give forces directed only along that direction. This result follows directly from the orthogonality properties of eigenvectors of symmetric matrices [83]. *The important conclusion is that, even for a particle of arbitrary shape, there is a natural choice for the coordinate axes.*

2. The angle θ_{UF} between $\boldsymbol{U}$ and $\boldsymbol{F}$ is obtuse. This follows from the energy dissipation argument, $-\boldsymbol{U} \cdot \boldsymbol{F} = -|\boldsymbol{U}|\,|\boldsymbol{F}| \cos\theta_{UF} > 0$.

3. Given $\boldsymbol{A} \cdot \boldsymbol{v}_i = A_i \boldsymbol{v}_i$, *i.e.*, the drag is colinear along three directions $\boldsymbol{v}_i$, and no pair of which are mutually orthogonal, except perhaps one pair. Then $\boldsymbol{A}$ is isotropic. Proof: Take $\boldsymbol{v}_1$ and $\boldsymbol{v}_2$ with $\boldsymbol{v}_1 \cdot \boldsymbol{v}_2 \neq 0$. We have $A_1 \boldsymbol{v}_1 \cdot \boldsymbol{v}_2 = \boldsymbol{v}_2 \cdot \boldsymbol{A} \cdot \boldsymbol{v}_1 = \boldsymbol{v}_1 \cdot \boldsymbol{A} \cdot \boldsymbol{v}_2 = A_2 \boldsymbol{v}_1 \cdot \boldsymbol{v}_2$, which forces $A_1 = A_2$ if $\boldsymbol{v}_1 \cdot \boldsymbol{v}_2 \neq 0$. This is a direct way of establishing that regular polyhedra (the Platonic solids) have isotropic resistance tensor $\boldsymbol{A}$.

Similar conclusions may be derived for the rotational resistance tensor $\boldsymbol{C}$.

5.2.2 The Hydrodynamic Center of Resistance

Consider the axisymmetric pear-shaped object of Figure 5.1. For transverse translations, there will be a torque exerted in the direction $\boldsymbol{U} \times \boldsymbol{d}$, the exact magnitude (and sign) of the torque depending on the choice of the center. This is readily apparent from the figure, as we move the center along the axis from point P to Q. At some point between P and Q, (the hydrodynamic center) we expect the torque to vanish. The skew-shaped propeller in the same figure also experiences a torque when it is moved (without rotation) along the axial direction. Here, however, the hydrodynamic torque is in the axial direction, so a shift in the center along the axis has no effect on the torque, so there is no point for which the coupling tensor $\boldsymbol{B}$ vanishes. On the other hand, the centroid is still a special point, because there the coupling tensor is symmetric. This is most readily seen by observing that translations along the axial direction and any transverse direction give torques in the same direction as the motion. Thus the tensor has three orthogonal principal directions. We will see below that the hydrodynamic center exists for particles of arbitrary shape and that it is unique. We note that if $\boldsymbol{B}$ vanishes at some point, it can do so only at that point, for this is simply a special case of the coupling tensor being symmetric.[3]

[3]In the original work [10] vanishing of $\boldsymbol{B}$ is given as the condition for the hydrodynamic center. The more complete result and proof given here follow those given in the later work [35], which first appeared in 1965.

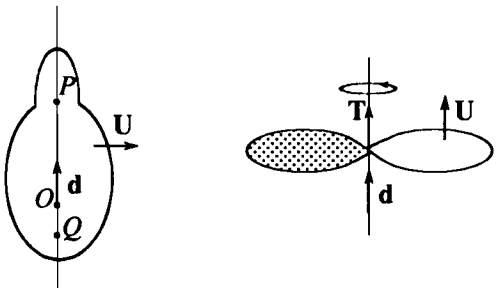

Figure 5.1: Hydrodynamic centers of resistance: an axisymmetric body and a propeller.

This discussion then motivates a search for the "natural origin" for a particle of arbitrary shape to complement the natural coordinate directions found above.

Consider a particle undergoing just translational motion and the resulting torques $\boldsymbol{T}(\boldsymbol{x}_1)$ and $\boldsymbol{T}(\boldsymbol{x}_2)$ with respect to two centers $\boldsymbol{x}_1$ and $\boldsymbol{x}_2$. The difference is calculated as

$$\begin{aligned}\boldsymbol{T}(\boldsymbol{x}_2) - \boldsymbol{T}(\boldsymbol{x}_1) &= \oint_{S_p} (\boldsymbol{x} - \boldsymbol{x}_2) \times (\boldsymbol{\sigma} \cdot \hat{\boldsymbol{n}})\, dS - \oint_{S_p} (\boldsymbol{x} - \boldsymbol{x}_1) \times (\boldsymbol{\sigma} \cdot \hat{\boldsymbol{n}})\, dS \\ &= \oint_{S_p} (\boldsymbol{x}_1 - \boldsymbol{x}_2) \times (\boldsymbol{\sigma} \cdot \hat{\boldsymbol{n}})\, dS \\ &= (\boldsymbol{x}_1 - \boldsymbol{x}_2) \times \boldsymbol{F} \ ,\end{aligned}$$

or in terms of the coupling tensor,

$$B_{ij}^{(2)} = B_{ij}^{(1)} - \epsilon_{ikl}(\boldsymbol{x}_2 - \boldsymbol{x}_1)_k A_{lj} \ .$$

Here, the superscripts on the coupling tensor denote the respective centers. Suppose that at $\boldsymbol{x}_2 = \boldsymbol{x}_{cr}$ (this will be the hydrodynamic center of resistance) $\boldsymbol{B}^{(cr)}$ is symmetric, so that the antisymmetric part of the previous equation becomes

$$B_{ij}^{(1)} - B_{ji}^{(1)} = \epsilon_{ikl}(\boldsymbol{x}_{cr} - \boldsymbol{x}_1)_k A_{lj} - \epsilon_{jkl}(\boldsymbol{x}_{cr} - \boldsymbol{x}_1)_k A_{li} \ . \tag{5.10}$$

To obtain an explicit expression for the hydrodynamic center of resistance, we apply ϵ_{mij} to both sides and use

$$\epsilon_{mij}\epsilon_{ikl} = \delta_{jk}\delta_{lm} - \delta_{jl}\delta_{km} \ , \qquad \epsilon_{mij}\epsilon_{jkl} = \delta_{km}\delta_{il} - \delta_{lm}\delta_{ik} \ ,$$

to arrive at

$$\left[(\boldsymbol{A} - (\mathrm{tr}\boldsymbol{A})\boldsymbol{\delta}) \cdot (\boldsymbol{x}_{cr} - \boldsymbol{x}_1)\right]_m = \frac{1}{2}\epsilon_{mij}\left[B_{ij}^{(1)} - B_{ji}^{(1)}\right] \ .$$

The matrix associated with $\boldsymbol{A} - (\mathrm{tr}\boldsymbol{A})\boldsymbol{\delta}$ is always nonsingular. In fact, with the principal directions $\boldsymbol{e}_i$, $i = 1, 2, 3$ as basis, $\boldsymbol{A}$ is diagonal and the matrix in

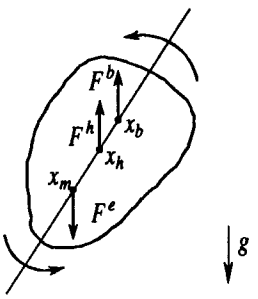

Figure 5.2: The couples acting on a settling body.

question has the representation

$$\boldsymbol{A} - (\mathrm{tr}\boldsymbol{A})\boldsymbol{\delta} = -\begin{pmatrix} A_2 + A_3 & 0 & 0 \\ 0 & A_3 + A_1 & 0 \\ 0 & 0 & A_1 + A_2 \end{pmatrix},$$

where $A_i > 0$, $i = 1, 2, 3$ are the principal values. The determinant, $|\boldsymbol{A} - (\mathrm{tr}\boldsymbol{A})\boldsymbol{\delta}|$, cannot vanish, and the explicit expression for the hydrodynamic center follows as

$$\boldsymbol{x}_{cr} - \boldsymbol{x}_1 = \frac{1}{2}\left((\mathrm{tr}\boldsymbol{A})\boldsymbol{\delta} - \boldsymbol{A}\right)^{-1} \cdot \left[\boldsymbol{\epsilon} : \left(\boldsymbol{B}^{(1)} - \boldsymbol{B}^{t(1)}\right)\right] .$$

In terms of the principal axes of $\boldsymbol{A}$, this relation may be written as

$$\begin{aligned} \boldsymbol{x}_{cr} - \boldsymbol{x}_1 &= \frac{B^{(1)}_{32} - B^{(1)}_{23}}{(A_2 + A_3)}\boldsymbol{e}_1 + \frac{B^{(1)}_{13} - B^{(1)}_{31}}{(A_3 + A_1)}\boldsymbol{e}_2 \\ &+ \frac{B^{(1)}_{21} - B^{(1)}_{12}}{(A_1 + A_2)}\boldsymbol{e}_3 . \end{aligned} \tag{5.11}$$

Note that from the method of construction, the converse is readily demonstrated: At the hydrodynamic center of resistance, Equation 5.10 holds so that the coupling tensor is symmetric.

In summary, to locate the hydrodynamic center of resistance of a particle of arbitrary shape, we first determine the tensor $\boldsymbol{A}$, and then find its eigenvalues $\{A_1, A_2, A_3\}$ and principal directions $\{\boldsymbol{e}_1, \boldsymbol{e}_2, \boldsymbol{e}_3\}$. We then pick *any* convenient point $\boldsymbol{x}_1$ and calculate the coupling tensor $\boldsymbol{B}(\boldsymbol{x}_1)$ between the translation velocity and the torque with respect to that point. Equation 5.11 gives the location of the hydrodynamic center relative to $\boldsymbol{x}_1$. Although the reference point appears in the formulae, it is easily verified that the hydrodynamic center is well defined and independent of the choice for $\boldsymbol{x}_1$ (see Exercises 5.2 and 5.3).

For an illustration of the use of the hydrodynamic center, consider an axisymmetric solid object of nonuniform density distribution (see Figure 5.2). (Another illustration is given later in the chapter.) In general, the hydrodynamic center, $\boldsymbol{x}_{cr}$, the center of buoyancy (center of mass of the displaced fluid),

$\boldsymbol{x}_b$, and center of mass, $\boldsymbol{x}_m$, are different, as shown in Figure 5.2. Also, while the first two are purely geometric entities determined by the surface geometry, the third center depends on the details of the mass distribution within the body. The rigid-body rotation of the particle as it settles under the influence of gravity can be determined by balancing all three couples on the body, with the forces placed at the appropriate centers.

5.2.3 Translation Theorems for Resistance Tensors

In the preceding discussion, we saw that the coupling tensor depended on the choice of the center in the calculation of the hydrodynamic torque. Consider two different parametrizations of a rigid-body motion, $\boldsymbol{U}_1 + \boldsymbol{\omega} \times (\boldsymbol{x} - \boldsymbol{x}_1) = \boldsymbol{U}_2 + \boldsymbol{\omega} \times (\boldsymbol{x} - \boldsymbol{x}_2)$, with the torques in each case measured relative to the center of rotation. The so-called translation theorems [35] furnish the relation between tensors defined using the different origins:

$$\begin{aligned} \boldsymbol{A}^{(2)} &= \boldsymbol{A}^{(1)} = \boldsymbol{A} \\ \boldsymbol{B}^{(2)} &= \boldsymbol{B}^{(1)} - (\boldsymbol{x}_2 - \boldsymbol{x}_1) \times \boldsymbol{A} \\ \boldsymbol{C}^{(2)} &= \boldsymbol{C}^{(1)} - (\boldsymbol{x}_2 - \boldsymbol{x}_1) \times \boldsymbol{A} \times (\boldsymbol{x}_2 - \boldsymbol{x}_1) \\ &+ \boldsymbol{B}^{(1)} \times (\boldsymbol{x}_2 - \boldsymbol{x}_1) - (\boldsymbol{x}_2 - \boldsymbol{x}_1) \times \boldsymbol{B}^{t(1)} . \end{aligned}$$

These identities are readily established using arguments encountered in the derivation of the hydrodynamic center. The translation theorems are quite useful, as we will see later. In the following section, we consider the resistance tensors of a "composite" particle formed by joining simpler units. The tensor for the composite particle can be constructed from those of the units by applying the translation theorems. In Part IV, we will encounter hydrodynamic calculations with respect to centers dictated by the mathematical analysis, while the interpretation of the results and subsequent physical applications are most natural at the hydrodynamic center. The translation theorems provide the needed linkage.

5.3 The Mobility Tensor

Many physical problems in microhydrodynamics require the solution of the motion of the particle in response to prescribed forces and torques in a known ambient flow. We call such situations *mobility* problems. We can invoke linearity again to write

$$\begin{pmatrix} \boldsymbol{U}^\infty - \boldsymbol{U} \\ \boldsymbol{\Omega}^\infty - \boldsymbol{\omega} \\ \mu^{-1}\boldsymbol{S} \end{pmatrix} = \begin{pmatrix} \boldsymbol{a} & \tilde{\boldsymbol{b}} & \tilde{\boldsymbol{g}} \\ \boldsymbol{b} & \boldsymbol{c} & \tilde{\boldsymbol{h}} \\ \boldsymbol{g} & \boldsymbol{h} & \boldsymbol{m} \end{pmatrix} \begin{pmatrix} \mu^{-1}\boldsymbol{F} \\ \mu^{-1}\boldsymbol{T} \\ \boldsymbol{E}^\infty \end{pmatrix} . \tag{5.12}$$

The square matrix is the *mobility matrix*; it contains second-rank tensors $\boldsymbol{a}$, $\boldsymbol{b}$, and $\boldsymbol{c}$, third-rank tensors $\boldsymbol{g}$ and $\boldsymbol{h}$, and a fourth-rank tensor $\boldsymbol{m}$. The fluid viscosity has been scaled from these quantities so that the matrix elements

have dimensions of length to the -1 (a), -2 (b), -3 (c), zero (h), first (g), and third (m) powers.

The elements of the mobility matrix also obey symmetry relations as a consequence of the Lorentz reciprocal theorem:

$$\begin{aligned} a_{ij} &= a_{ji} \ , \qquad c_{ij} = c_{ji} \ , \qquad m_{ijkl} = m_{klij} \ , \\ b_{ij} &= \tilde{b}_{ji} \ , \qquad g_{ijk} = -\tilde{g}_{kij} \ , \qquad h_{ijk} = -\tilde{h}_{kij} \ . \end{aligned}$$

Note the occurrence of minus signs in the relations for $\boldsymbol{g}$ and $\boldsymbol{h}$. The proofs for symmetry are similar to the ones for the resistance matrix (see Exercise 5.1). For example, the relation for $\boldsymbol{h}$ can be derived as follows. We start with Equation 5.2 and take for $\boldsymbol{v}_1$ the disturbance field of a *force-free, torque-free particle fixed in a straining motion* $\boldsymbol{E}^\infty \cdot \boldsymbol{x}$. For $\boldsymbol{v}_2$, we choose the disturbance field generated by a force-free particle, with external torque $-\boldsymbol{T}$ in a quiescent fluid. Of course, our choices for $\boldsymbol{v}_1$ and $\boldsymbol{v}_2$ are dictated by the definitions of $\boldsymbol{h}$ and $\tilde{\boldsymbol{h}}$. These two velocity fields vanish at infinity, while on the particle surface the boundary conditions are

$$\boldsymbol{v}_1(\boldsymbol{x}) = -\boldsymbol{E}^\infty \cdot \boldsymbol{x} + \boldsymbol{U}_1 + \boldsymbol{\omega}_1 \times \boldsymbol{x} \ , \qquad \boldsymbol{v}_2(\boldsymbol{x}) = \boldsymbol{U}_2 + \boldsymbol{\omega}_2 \times \boldsymbol{x} \ .$$

The rotational velocity $\boldsymbol{\omega}_1$ and stresslet $\boldsymbol{S}_2$ in these two flows follow from the definitions of the mobility functions as

$$(\boldsymbol{\omega}_1)_k = -\tilde{h}_{kij} E^\infty_{ij}$$

and

$$(\boldsymbol{S}_2)_{ij} = h_{ijk} (\boldsymbol{T}_2)_k \ .$$

We apply the reciprocal theorem over the same fluid region as before. One side of the equation simplifies as

$$\begin{aligned} -\oint_S (\boldsymbol{v}_1)_i (\boldsymbol{\sigma}_2 \cdot \boldsymbol{n})_i \, dS &= \oint_S \left[E^\infty_{ij} x_j - (\boldsymbol{U}_1)_i - (\boldsymbol{\omega}_1 \times \boldsymbol{x})_i \right] (\boldsymbol{\sigma}_2 \cdot \boldsymbol{n})_i \, dS \\ &= E^\infty_{ij} (\boldsymbol{S}_2)_{ij} - (\boldsymbol{U}_1)_i (\boldsymbol{F}_2)_i - (\boldsymbol{\omega}_1)_i (\boldsymbol{T}_2)_i \\ &= E^\infty_{ij} h_{ijk} (\boldsymbol{T}_2)_k + \tilde{h}_{kij} E^\infty_{ij} (\boldsymbol{T}_2)_k \ . \end{aligned} \tag{5.13}$$

In the last step, we replaced $\boldsymbol{S}_2$ and $-\boldsymbol{\omega}_1$ with $\boldsymbol{h} \cdot \boldsymbol{T}_2$ and $\tilde{\boldsymbol{h}} : \boldsymbol{E}^\infty$, respectively, and we also used $\boldsymbol{F}_2 = \boldsymbol{0}$. The other side of the reciprocal relation simplifies as

$$\begin{aligned} -\oint_S (\boldsymbol{v}_2)_i (\boldsymbol{\sigma}_1 \cdot \boldsymbol{n})_i \, dS &= -\oint_S \left[(\boldsymbol{U}_2)_i + (\boldsymbol{\omega}_2 \times \boldsymbol{x})_i \right] (\boldsymbol{\sigma}_1 \cdot \boldsymbol{n})_i \, dS \\ &= -(\boldsymbol{U}_2)_i (\boldsymbol{F}_1)_i - (\boldsymbol{\omega}_2)_i (\boldsymbol{T}_1)_i \\ &= \boldsymbol{0} \ . \end{aligned} \tag{5.14}$$

Combining Equations 5.13 and 5.14 gives, since $\boldsymbol{T}_2$ and $\boldsymbol{E}$ are arbitrary constants, $h_{ijk} = -\tilde{h}_{kij}$, as claimed.

5.3.1 Translation Theorems for Mobility Tensors

The translation theorems for the mobility tensor are as follows:

$$\begin{aligned} \boldsymbol{a}^{(2)} &= \boldsymbol{a}^{(1)} - (\boldsymbol{x}_2 - \boldsymbol{x}_1) \times \boldsymbol{c} \times (\boldsymbol{x}_2 - \boldsymbol{x}_1) - (\boldsymbol{x}_2 - \boldsymbol{x}_1) \times \boldsymbol{b}^{(1)} + \boldsymbol{b}^{t(1)} \times (\boldsymbol{x}_2 - \boldsymbol{x}_1) \\ \boldsymbol{b}^{(2)} &= \boldsymbol{b}^{(1)} + \boldsymbol{c} \times (\boldsymbol{x}_2 - \boldsymbol{x}_1) \\ \boldsymbol{c}^{(2)} &= \boldsymbol{c}^{(1)} = \boldsymbol{c} \, . \end{aligned}$$

If we compare this with the translation theorems for the resistance tensors, we see that the roles played by $\{\boldsymbol{a}, \boldsymbol{b}, \boldsymbol{b}^t, \boldsymbol{c}\}$ and $\{\boldsymbol{A}, \boldsymbol{B}, \boldsymbol{B}^t, \boldsymbol{C}\}$ are reversed.

5.3.2 The Hydrodynamic Center of Mobility

Here, we correct a widely-held misconception and show that the hydrodynamic center for the mobility tensors in general differs from the hydrodynamic center of resistance. The hydrodynamic center for the mobility, $\boldsymbol{x}_{cm}$, is given by a relation analogous to the one obtained earlier for the resistance tensor:

$$\boldsymbol{x}_{cm} - \boldsymbol{x}_1 = \frac{b_{23}^{(1)} - b_{32}^{(1)}}{(c_2 + c_3)} \boldsymbol{e}_1 + \frac{b_{31}^{(1)} - b_{13}^{(1)}}{(c_3 + c_1)} \boldsymbol{e}_2 + \frac{b_{12}^{(1)} - b_{21}^{(1)}}{(c_1 + c_2)} \boldsymbol{e}_3 \, .$$

This result can also be deduced from the corresponding result for the resistance formulation, by reversing the roles played by $\{\boldsymbol{a}, \boldsymbol{b}, \boldsymbol{b}^t, \boldsymbol{c}\}$ and $\{\boldsymbol{A}, \boldsymbol{B}, \boldsymbol{B}^t, \boldsymbol{C}\}$.

The distance between the two hydrodynamic centers is obtained by solving the following relation[4]:

$$\mathbf{c}^{-1} \times (\boldsymbol{x}_{cm} - \boldsymbol{x}_{cr}) + (\boldsymbol{x}_{cm} - \boldsymbol{x}_{cr}) \times \mathbf{c}^{-1} = -\boldsymbol{\beta}^{(cr)} + \boldsymbol{\beta}^{t(cr)} \, ,$$

where $\boldsymbol{\beta}^{(cr)} = [\boldsymbol{C}\boldsymbol{A}^{-1}\boldsymbol{B}]^{(cr)}$ is a product of resistance tensors evaluated at the hydrodynamic center of resistance. Therefore, *the hydrodynamic centers of resistance and mobility coincide if and only if* $\boldsymbol{\beta}^{(cr)} = \boldsymbol{\beta}^{t(cr)}$. In terms of the principal directions and values of the mobility tensor, $\boldsymbol{c}$, the result is

$$\boldsymbol{x}_{cm} - \boldsymbol{x}_{cr} = \frac{\beta_{23}^{(cr)} - \beta_{32}^{(cr)}}{(c_2^{-1} + c_3^{-1})} \boldsymbol{e}_1 + \frac{\beta_{31}^{(cr)} - \beta_{13}^{(cr)}}{(c_3^{-1} + c_1^{-1})} \boldsymbol{e}_2 + \frac{\beta_{12}^{(cr)} - \beta_{21}^{(cr)}}{(c_1^{-1} + c_2^{-1})} \boldsymbol{e}_3 \, .$$

We interject a historical note here. Brenner's "proof" [13] that the hydrodynamic centers of resistance and mobility are coincident contains an error, equivalent to the erroneous conclusion that $\boldsymbol{\beta}$ is symmetric for all particle shapes. Bernal and de la Torre [6] and Wegener [90] appear to have been the first to (independently) notice this error. These studies of the diffusivity of proteins required mobility calculations of bent and hinged rods, and for such objects $\boldsymbol{\beta}$ is not symmetric. Later in this chapter, we will examine other shapes for which this is also the case.

[4]We thank Douglas Brune for bringing this relation to our attention.

5.4 Relations Between the Resistance and Mobility Tensors

Clearly, the resistance and mobility formulations are related and but for $\boldsymbol{S}$ appearing as a dependent variable in both problems, the two formulations would be formal inverses of each other. The force and torque portion of the resistance equation may be written as

$$\begin{aligned}\begin{pmatrix} \boldsymbol{F} \\ \boldsymbol{T} \end{pmatrix} &= \mu \begin{pmatrix} \boldsymbol{A} & \tilde{\boldsymbol{B}} \\ \boldsymbol{B} & \boldsymbol{C} \end{pmatrix} \begin{pmatrix} \boldsymbol{U}^{\infty} - \boldsymbol{U} \\ \boldsymbol{\Omega}^{\infty} - \boldsymbol{\omega} \end{pmatrix} + \mu \begin{pmatrix} \tilde{\boldsymbol{G}} \\ \tilde{\boldsymbol{H}} \end{pmatrix} \begin{pmatrix} \boldsymbol{E}^{\infty} \end{pmatrix} \\ &= \mu \begin{pmatrix} \boldsymbol{A} & \tilde{\boldsymbol{B}} \\ \boldsymbol{B} & \boldsymbol{C} \end{pmatrix} \left[\begin{pmatrix} \boldsymbol{a} & \tilde{\boldsymbol{b}} \\ \boldsymbol{b} & \boldsymbol{c} \end{pmatrix} \begin{pmatrix} \mu^{-1}\boldsymbol{F} \\ \mu^{-1}\boldsymbol{T} \end{pmatrix} + \begin{pmatrix} \tilde{\boldsymbol{g}} \\ \tilde{\boldsymbol{h}} \end{pmatrix} \begin{pmatrix} \boldsymbol{E}^{\infty} \end{pmatrix} \right] \\ &\quad + \mu \begin{pmatrix} \tilde{\boldsymbol{G}} \\ \tilde{\boldsymbol{H}} \end{pmatrix} \begin{pmatrix} \boldsymbol{E}^{\infty} \end{pmatrix} , \end{aligned} \tag{5.15}$$

which implies that

$$\begin{pmatrix} \boldsymbol{A} & \tilde{\boldsymbol{B}} \\ \boldsymbol{B} & \boldsymbol{C} \end{pmatrix} \begin{pmatrix} \boldsymbol{a} & \tilde{\boldsymbol{b}} \\ \boldsymbol{b} & \boldsymbol{c} \end{pmatrix} = \begin{pmatrix} \boldsymbol{\delta} & \boldsymbol{0} \\ \boldsymbol{0} & \boldsymbol{\delta} \end{pmatrix} \tag{5.16}$$

and

$$\begin{pmatrix} \boldsymbol{A} & \tilde{\boldsymbol{B}} \\ \boldsymbol{B} & \boldsymbol{C} \end{pmatrix} \begin{pmatrix} \tilde{\boldsymbol{g}} \\ \tilde{\boldsymbol{h}} \end{pmatrix} + \begin{pmatrix} \tilde{\boldsymbol{G}} \\ \tilde{\boldsymbol{H}} \end{pmatrix} = \begin{pmatrix} \boldsymbol{0} \\ \boldsymbol{0} \end{pmatrix} . \tag{5.17}$$

In a similar manner, the resistance expression for the stresslet may be combined with the mobility expressions to obtain relations for $\boldsymbol{g}$, $\boldsymbol{h}$, and $\boldsymbol{m}$ in terms of the resistance tensors. The complete set of relations follows as

$$\begin{pmatrix} \boldsymbol{a} & \tilde{\boldsymbol{b}} \\ \boldsymbol{b} & \boldsymbol{c} \end{pmatrix} = \begin{pmatrix} \boldsymbol{A} & \tilde{\boldsymbol{B}} \\ \boldsymbol{B} & \boldsymbol{C} \end{pmatrix}^{-1} \tag{5.18}$$

$$\begin{pmatrix} \tilde{\boldsymbol{g}} \\ \tilde{\boldsymbol{h}} \end{pmatrix} = -\begin{pmatrix} \boldsymbol{A} & \tilde{\boldsymbol{B}} \\ \boldsymbol{B} & \boldsymbol{C} \end{pmatrix}^{-1} \begin{pmatrix} \tilde{\boldsymbol{G}} \\ \tilde{\boldsymbol{H}} \end{pmatrix} \tag{5.19}$$

$$\begin{pmatrix} \boldsymbol{g} & \boldsymbol{h} \end{pmatrix} = \begin{pmatrix} \boldsymbol{G} & \boldsymbol{H} \end{pmatrix} \begin{pmatrix} \boldsymbol{A} & \tilde{\boldsymbol{B}} \\ \boldsymbol{B} & \boldsymbol{C} \end{pmatrix}^{-1} \tag{5.20}$$

$$\boldsymbol{m} = \boldsymbol{M} - \begin{pmatrix} \boldsymbol{G} & \boldsymbol{H} \end{pmatrix} \begin{pmatrix} \boldsymbol{A} & \tilde{\boldsymbol{B}} \\ \boldsymbol{B} & \boldsymbol{C} \end{pmatrix}^{-1} \begin{pmatrix} \tilde{\boldsymbol{G}} \\ \tilde{\boldsymbol{H}} \end{pmatrix} . \tag{5.21}$$

Note that the stresslet on a particle when the particle is force-free and torque-free is in general different from that when it is stationary. In fact, using energy dissipation arguments, we may state $\boldsymbol{m} \leq \boldsymbol{M}$.

Some further reduction is possible, using inversion relations for block matrices. The explicit results for the mobility tensors $\boldsymbol{a}$, $\boldsymbol{b}$, and $\boldsymbol{c}$ are

$$\boldsymbol{a} = (\boldsymbol{A} - \boldsymbol{B}^t\boldsymbol{C}^{-1}\boldsymbol{B})^{-1} \tag{5.22}$$

$$\boldsymbol{b} = -\boldsymbol{C}^{-1}\boldsymbol{B}(\boldsymbol{A} - \boldsymbol{B}^t\boldsymbol{C}^{-1}\boldsymbol{B})^{-1} \tag{5.23}$$

$$\boldsymbol{c} = (\boldsymbol{C} - \boldsymbol{B}\boldsymbol{A}^{-1}\boldsymbol{B}^t)^{-1} . \tag{5.24}$$

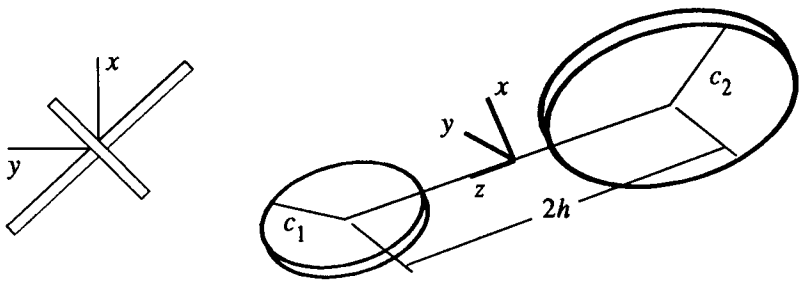

Figure 5.3: A propeller with unequal blades.

In principle, when faced with a mobility problem, we may proceed by first solving an appropriate set of resistance problems for which the particle motions are prescribed (boundary conditions are specified) and then use the relations above to obtain the mobility functions. For many-body problems, this approach is feasible in principle, but infeasible in practice — the computational costs are prohibitive. Furthermore, with respect to the gap width, the resistance functions diverge in a singular fashion as contact is approached (see Chapter 9), so the resistance matrix becomes ill-conditioned, *i.e.*, hard to invert numerically. For this reason, we will devote some effort in later chapters to the issue of direct solution of mobility problems.

We conclude this section with an example calculation of the resistance and mobility tensors of a "propeller" formed by attaching two thin circular disks to a frictionless rod, in the skew-symmetric fashion, pitched at an angle of 90° to each other, as shown in Figure 5.3. The center-to-center distance along the rod will be denoted by $2h$. We generalize the original treatment in Happel and Brenner [35] (pp. 179–180) by taking disks of different sizes, which introduces a key asymmetry in the problem that is necessary to demonstrate that the hydrodynamic centers of resistance and mobility are distinct. We will neglect hydrodynamic interactions between the disks, a good assumption if h is great compared to the disk radii.

In the first step, we write the resistance tensor with respect to an origin taken at the midpoint between the disk centers. The resistance tensor for the composite object is most easily computed by applying the translation theorems to the resistances of each disk, *i.e.*, shifting the reference point for each resistance tensor from the disk centers O_1 and O_2 to the midpoint, O. If the disk radii are $c_1 = c$ and $c_2 = 3c$ (this choice leads to nice numbers in the subsequent illustration; a general treatment is of little interest), and lengths are scaled

with c, the resistance tensors become:

$$\begin{pmatrix} \boldsymbol{A} & \boldsymbol{B}^t \\ \boldsymbol{B} & \boldsymbol{C} \end{pmatrix} = \frac{16}{3} \left(\begin{array}{ccc|ccc} 10 & 1 & 0 & 2h & -5h & 0 \\ 1 & 10 & 0 & 5h & -2h & 0 \\ 0 & 0 & 8 & 0 & 0 & 0 \\ \hline 2h & 5h & 0 & 56+10h^2 & -h^2 & 0 \\ -5h & -2h & 0 & -h^2 & 56+10h^2 & 0 \\ 0 & 0 & 0 & 0 & 0 & 56 \end{array}\right).$$

The symmetry of the overall matrix and the submatrices on the diagonal blocks is in accordance with the general theory.

We find that the eigenvalues and eigenvectors of the matrix representing the resistance tensor $\boldsymbol{A}$ are $8, 9, 11$, and

$$\begin{pmatrix} 1/\sqrt{2} \\ -1/\sqrt{2} \\ 0 \end{pmatrix}, \quad \begin{pmatrix} 1/\sqrt{2} \\ 1/\sqrt{2} \\ 0 \end{pmatrix}, \quad \begin{pmatrix} 0 \\ 0 \\ 1 \end{pmatrix}.$$

We may diagonalize $\boldsymbol{A}$ by using the orthogonal matrix Q with columns consisting of the eigenvectors above. In the new coordinate system, the matrices are given by $Q^t\boldsymbol{A}Q$, $Q^t\boldsymbol{B}Q$, *etc.*, and the grand resistance matrix becomes

$$\frac{16}{3} \left(\begin{array}{ccc|ccc} 9 & 0 & 0 & 0 & 0 & 0 \\ 0 & 11 & 0 & 7h & -3h & 0 \\ 0 & 0 & 8 & 0 & 0 & 0 \\ \hline 0 & 7h & 0 & 56+11h^2 & 0 & 0 \\ 0 & -3h & 0 & 0 & 56+11h^2 & 0 \\ 0 & 0 & 0 & 0 & 0 & 56 \end{array}\right).$$

In this example, the principal directions of $\boldsymbol{A}$ and $\boldsymbol{C}$ just happen to coincide, so that $\boldsymbol{C}$ is diagonalized as well.

We continue the example by locating the hydrodynamic center (for disks of equal size, the center would be at the midpoint). Using Equation 5.11, we find $\boldsymbol{x}_{cr} = -(7/20)\boldsymbol{e}_3$, and after applying the translation theorems for the resistance tensors, we arrive at

$$\frac{16}{3} \left(\begin{array}{ccc|ccc} 9 & 0 & 0 & 0 & \frac{63}{20}h & 0 \\ 0 & 11 & 0 & \frac{63}{20}h & -3h & 0 \\ 0 & 0 & 8 & 0 & 0 & 0 \\ \hline 0 & \frac{63}{20}h & 0 & 56+\frac{2979}{400}h^2 & \frac{21}{20}h^2 & 0 \\ \frac{63}{20}h & -3h & 0 & \frac{21}{20}h^2 & 56+\frac{4041}{400}h^2 & 0 \\ 0 & 0 & 0 & 0 & 0 & 56 \end{array}\right)$$

for rotations and torques about the hydrodynamic center of resistance. The coupling tensor $\boldsymbol{B}^{(cr)}$ is now symmetric, as required by the general theory. The

following result for the coupling tensor $\boldsymbol{b}$ with respect to $\boldsymbol{x}_{cr}$ can be derived by using Equation 5.24,

$$\boldsymbol{b} = \frac{1}{D(h)} \begin{pmatrix} 147h^3 & -18h(35h^2+196) & 0 \\ -56h(9h^2+77) & 3h(171h^2+1120) & 0 \\ 0 & 0 & 0 \end{pmatrix} ,$$

where $D(h) = 20(549h^4 + 9072h^2 + 34496)$ and $\boldsymbol{b}$ *is not symmetric*, since $\boldsymbol{x}_{cm} \neq \boldsymbol{x}_{cr}$ for this object. Both hydrodynamic centers are located on the side of the rod closer to the bigger disk. For the limiting case of $h \gg 1$, we have

$$\begin{aligned} \boldsymbol{x}_{cr} &= -0.175h\boldsymbol{e}_3 \\ \boldsymbol{x}_{cm} &= -0.408h\boldsymbol{e}_3 , \end{aligned}$$

and the distance between the two hydrodynamic centers is approximately $0.233h$.

5.5 Axisymmetric Particles

5.5.1 General Resistance Formulation in a Linear Field

For axisymmetric shapes, we obtain further reductions in the algebraic structure of the resistance and mobility problems. Perhaps the simplest manifestation of this statement concerns the drag coefficient on a translating particle. This coefficient will take on the same values for translations in the two directions transverse to the axis of symmetry. If the coordinate system is chosen so that the z-axis is along this axis of symmetry, then the resistance relation becomes

$$\begin{aligned} F_1 &= \mu A^{\perp}(U_1^{\infty} - U_1) \\ F_2 &= \mu A^{\perp}(U_2^{\infty} - U_2) \\ F_3 &= \mu A^{\parallel}(U_3^{\infty} - U_3) , \end{aligned}$$

where $A_{33} = A^{\parallel}$ and $A_{11} = A_{22} = A^{\perp}$. Net translation along one of the coordinate directions gives a force component in only that direction, due to symmetry. The equality of the resistances in the x- and y-directions is also a consequence of the symmetry in the particle shape.

Before proceeding further, we digress here to introduce a slight generalization in the notation. We do this because in later chapters we will want to align coordinate axes to suit other considerations such as the direction of external fields, *etc.* If we denote the particle symmetry axis with the unit vector $\boldsymbol{d}$, then in the preceding equations $\boldsymbol{e}_z = \boldsymbol{d}$ and every occurrence of $\boldsymbol{e}_x\boldsymbol{e}_x + \boldsymbol{e}_y\boldsymbol{e}_y$ may be replaced with $\boldsymbol{\delta} - \boldsymbol{dd}$. Thus, the resistance relation may be written as

$$\boldsymbol{F} = \mu \left[A^{\parallel}\boldsymbol{dd} + A^{\perp}(\boldsymbol{\delta} - \boldsymbol{dd}) \right] \cdot (\boldsymbol{U}^{\infty} - \boldsymbol{U}) .$$

We may apply analogous operations on the set of resistance tensors to obtain

$$A_{ij} = X^A d_i d_j + Y^A(\delta_{ij} - d_i d_j) \tag{5.25}$$

$$B_{ij} = Y^B \epsilon_{ijk} d_k \tag{5.26}$$

$$C_{ij} = X^C d_i d_j + Y^C(\delta_{ij} - d_i d_j) \tag{5.27}$$

$$G_{ijk} = X^G(d_i d_j - \frac{1}{3}\delta_{ij})d_k + Y^G(d_i\delta_{jk} + d_j\delta_{ik} - 2d_i d_j d_k) \tag{5.28}$$

$$H_{ijk} = \widetilde{H}_{kij} = Y^H(\epsilon_{ikl}d_j + \epsilon_{jkl}d_i)d_l \tag{5.29}$$

$$M_{ijkl} = X^M d^{(0)}_{ijkl} + Y^M d^{(1)}_{ijkl} + Z^M d^{(2)}_{ijkl} , \tag{5.30}$$

where

$$d^{(0)} = \frac{3}{2}(d_i d_j - \frac{1}{3}\delta_{ij})(d_k d_l - \frac{1}{3}\delta_{kl})$$

$$d^{(1)} = \frac{1}{2}(d_i\delta_{jl}d_k + d_j\delta_{il}d_k + d_i\delta_{jk}d_l + d_j\delta_{ik}d_l - 4d_i d_j d_k d_l)$$

$$d^{(2)} = \frac{1}{2}\delta_{ik}\delta_{jl} + \delta_{jk}\delta_{il} - \delta_{ij}\delta_{kl} + d_i d_j\delta_{kl} + \delta_{ij}d_k d_l$$
$$- d_i\delta_{jl}d_k - d_j\delta_{il}d_k - d_i\delta_{jk}d_l - d_j\delta_{ik}d_l + d_i d_j d_k d_l) ,$$

and X, Y, and Z are scalar resistance functions. The X functions are associated with axisymmetric problems, *e.g.*, $X^A = A^{\parallel}$, and the Y functions with transverse cases for the A and C tensors. More explicitly, if we use spherical coordinates about the particle axis $\boldsymbol{d}$, then the ambient flows in the resistance problems all have ϕ-dependences of the form $\exp(im\phi)$, as shown in Chapter 4. We assign X, Y, and Z to $m = 0$, ± 1, and ± 2, respectively.

The forms given in Equations 5.25–5.30 may be verified by considering $\boldsymbol{d} = \boldsymbol{e}_z$ and allowing for symmetry. For example, the coupling between translation and torque on an axisymmetric body is of the form $\boldsymbol{T} = -\mu Y^B \boldsymbol{U} \times \boldsymbol{d}$, and of course this coupling occurs only if we are interested in the torque about a point other than the hydrodynamic center. The analysis for $\boldsymbol{M}$ is more involved, and since it is perhaps less familiar to most readers, we consider it in some greater detail.

Example 5.1 The Resistance Tensor $\boldsymbol{M}$ for Axisymmetric Particles. We know that the rate-of-strain field $\boldsymbol{E}$ has five independent components because $E_{ij} = E_{ji}$ and $E_{jj} = 0$. For an axisymmetric particle with the axis of symmetry in the z-direction, we may select the following five rate-of-strain fields as the "basis":

$$\boldsymbol{E}^{(1)} = \begin{pmatrix} -1 & 0 & 0 \\ 0 & -1 & 0 \\ 0 & 0 & 2 \end{pmatrix} \qquad \boldsymbol{E}^{(2)} = \begin{pmatrix} 1 & 0 & 0 \\ 0 & -1 & 0 \\ 0 & 0 & 0 \end{pmatrix}$$

$$\boldsymbol{E}^{(3)} = \begin{pmatrix} 0 & 1 & 0 \\ 1 & 0 & 0 \\ 0 & 0 & 0 \end{pmatrix} \qquad \boldsymbol{E}^{(4)} = \begin{pmatrix} 0 & 0 & 1 \\ 0 & 0 & 0 \\ 1 & 0 & 0 \end{pmatrix}$$

$$\boldsymbol{E}^{(5)} = \begin{pmatrix} 0 & 0 & 0 \\ 0 & 0 & 1 \\ 0 & 1 & 0 \end{pmatrix} .$$

This may be shown explicitly by the following decomposition:

$$\boldsymbol{E} = \frac{1}{2}E_{zz}\boldsymbol{E}^{(1)} + \frac{1}{2}(E_{xx} - E_{yy})\boldsymbol{E}^{(2)} + E_{xy}\boldsymbol{E}^{(3)} + E_{xz}\boldsymbol{E}^{(4)} + E_{yz}\boldsymbol{E}^{(5)}.$$

Since $\boldsymbol{d} = \boldsymbol{e}_z$, the previous decomposition can be written as

$$E_{ij} = d^{(0)}_{ijkl}E_{kl} + d^{(1)}_{ijkl}E_{kl} + d^{(2)}_{ijkl}E_{kl} \ .$$

The $\boldsymbol{d}^{(0)}$ term corresponds to $(E_{zz}/2)\boldsymbol{E}^{(1)}$, the $\boldsymbol{d}^{(1)}$ term corresponds to $E_{xz}\boldsymbol{E}^{(4)} + E_{yz}\boldsymbol{E}^{(5)}$, and the last term corresponds to $\frac{1}{2}(E_{xx} - E_{yy})\boldsymbol{E}^{(2)} + E_{xy}\boldsymbol{E}^{(3)}$. Note that this decomposition actually holds for any tensor, because all terms canel except $\boldsymbol{E}$, but in general its usefulness is restricted to axisymmetric geometries.

The stresslet can also be decomposed in the same way, *i.e.*,

$$S_{ij} = d^{(0)}_{ijkl}S_{kl} + d^{(1)}_{ijkl}S_{kl} + d^{(2)}_{ijkl}S_{kl} \ . \tag{5.31}$$

One can identify coordinate transformations that leave only one group invariant. Thus for each of the three groupings in the rate-of-strain field, assume initially that all three groupings of the stresslet expression are required and then show that the coefficients of the two "unwanted" groupings are zero.

For example, consider the rate-of-strain field

$$E_{ij} = d^{0}_{ijkl}E_{kl} \ ,$$

and first assume that the stresslet is of the general form in Equation 5.31. An arbitrary rotation by an angle ϕ about the z-axis has no effect on $\boldsymbol{d}^{(0)} : \boldsymbol{E}$ and $\boldsymbol{d}^{(0)} : \boldsymbol{S}$. However, $\boldsymbol{d}^{(m)} : \boldsymbol{S}$, $m = 1, 2$ contains factors of $\cos m\phi$ and $\sin m\phi$, thus the equality is possible only if these terms are absent. Analogous arguments apply for the other rate-of-strain fields and thus the final result is obtained.$\Diamond$

5.5.2 A Torque-Free Axisymmetric Particle in a Linear Field: The Jeffery Orbits

We generalize the result derived earlier in this chapter, concerning the rotation of a prolate spheroid in a linear field, to the more general case of any axisymmetric particle in a linear field. Again, we set $\boldsymbol{T} = \boldsymbol{0}$ in the expression for the torque and dot multiply through with the dyad:

$$\left[(X^C)^{-1}\boldsymbol{dd} + (Y^C)^{-1}(\boldsymbol{\delta} - \boldsymbol{dd})\right] \ .$$

Again, we find that the rotational motion follows as

$$\boldsymbol{\omega} \times \boldsymbol{x} = \boldsymbol{\Omega}^{\infty} \times \boldsymbol{x} + \left(\frac{Y^H}{Y^C}\right)\left[\boldsymbol{E}^{\infty} \cdot \boldsymbol{d}\,(\boldsymbol{d} \cdot \boldsymbol{x}) - \boldsymbol{E}^{\infty} : \boldsymbol{xd}\,\boldsymbol{d}\right] \ . \tag{5.32}$$

Thus the general axisymmetric particle rotates with the angular velocity of the ambient fluid, plus a contribution from the rate-of-strain field that acts to align the axis along a principal direction of $\boldsymbol{E}$. The relative importance of the

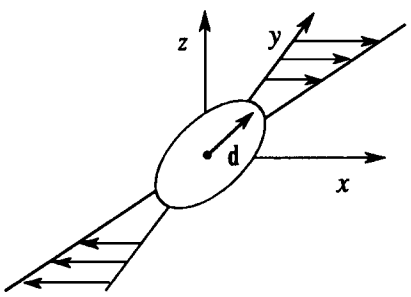

Figure 5.4: An axisymmetric particle in a shear field.

alignment effect depends on the aspect ratio: It becomes less important for nearly spherical shapes. In fact, the Bretherton constant, $B = Y^H/Y^C$ may be viewed as a hydrodynamic measure of nonsphericity. For ellipsoids of revolution with aspect ratio r, we recall that $B = (r^2 - 1)/(r^2 + 1)$, and thus $B > 0$ for prolate objects, $B = 0$ for a sphere,[5] and $B < 0$ for an oblate object. For what axisymmetric shapes would we expect $|B| \leq 1$?

We now consider the special case of a neutrally buoyant torque-free axisymmetric particle in the shear field $\boldsymbol{v}^\infty = \dot{\gamma} y \boldsymbol{e}_1$. The orientation of the particle axis $\boldsymbol{d}$ is parametrized using spherical polar coordinates so that

$$\begin{aligned} d_1 &= \sin\theta\cos\phi \\ d_2 &= \sin\theta\sin\phi \\ d_3 &= \cos\theta \ . \end{aligned}$$

The geometry is depicted in Figure 5.4. For this flow field, the ambient rotation and rate-of-strain are given by

$$\boldsymbol{\Omega}^\infty = -\frac{1}{2}\dot{\gamma}\boldsymbol{e}_3 \ , \qquad \boldsymbol{E}^\infty = \frac{\dot{\gamma}}{2}\begin{pmatrix} 0 & 1 & 0 \\ 1 & 0 & 0 \\ 0 & 0 & 0 \end{pmatrix} \ .$$

The time evolution of the particle orientation, $\dot{\boldsymbol{d}}$, is obtained from the general mobility relation for the rotation of an axisymmetric particle in a linear field, Equation 5.32, by simply replacing $\boldsymbol{x} \to \boldsymbol{d}$:

$$\dot{\boldsymbol{d}} = \boldsymbol{\omega} \times \boldsymbol{d} = \boldsymbol{\Omega}^\infty \times \boldsymbol{d} + B(\boldsymbol{E}^\infty \cdot \boldsymbol{d} - \boldsymbol{E}^\infty : \boldsymbol{dd}\,\boldsymbol{d}) \ . \tag{5.33}$$

For the shear flow, the various terms simplify as

$$\boldsymbol{\Omega}^\infty \times \boldsymbol{d} \ = \ \frac{\dot{\gamma}}{2}(d_2\boldsymbol{e}_1 - d_1\boldsymbol{e}_2)$$

[5] And any other particle that experiences no torque when kept fixed in a rate-of-strain field.

$$\begin{aligned} \boldsymbol{E}^{\infty} \cdot \boldsymbol{d} &= \frac{\dot{\gamma}}{2}(d_2\boldsymbol{e}_1 + d_1\boldsymbol{e}_2) \\ \boldsymbol{E}^{\infty} : \boldsymbol{d}\boldsymbol{d}\boldsymbol{d} &= \dot{\gamma} d_1 d_2 (d_1\boldsymbol{e}_1 + d_2\boldsymbol{e}_2 + d_3\boldsymbol{e}_3) \ . \end{aligned}$$

To go from the equation for $\dot{\boldsymbol{d}}$ to equations for $\dot{\theta}$ and $\dot{\phi}$, we examine $\dot{d}_3$ and $d_1\dot{d}_2 - d_2\dot{d}_1$. From above, we have

$$\begin{aligned} \dot{d}_3 &= -\sin\theta\,\dot{\theta} = -B\dot{\gamma}\sin^2\theta\cos\theta\sin\phi\cos\phi \\ d_1\dot{d}_2 - d_2\dot{d}_1 &= \sin^2\theta\,\dot{\phi} = -\frac{\dot{\gamma}}{2}\sin^2\theta + B\frac{\dot{\gamma}}{2}\sin^2\theta(\sin^2\phi - \cos^2\phi) \ , \end{aligned}$$

or

$$\begin{aligned} \dot{\theta} &= -\left(\frac{r^2-1}{r^2+1}\right)\frac{\dot{\gamma}}{4}\sin 2\theta\,\sin 2\phi \\ \dot{\phi} &= \frac{-\dot{\gamma}}{r^2+1}(r^2\cos^2\phi + \sin^2\phi) \ . \end{aligned}$$

We have replaced the Bretherton constant by *defining* a hydrodynamic aspect ratio with $B = (r^2-1)/(r^2+1)$.

The differential equations may be solved exactly and yield periodic trajectories known as the *Jeffery orbits*,

$$\begin{aligned} \tan\theta &= \frac{Cr}{\left[r^2\cos^2\phi + \sin^2\phi\right]^{1/2}} \\ \tan\phi &= -r\tan\left(\frac{\dot{\gamma}t}{r+r^{-1}}\right) \ . \end{aligned}$$

The period $T = 2\pi(r + r^{-1})/\dot{\gamma}$ scales with the inverse shear rate and becomes longer with increasing nonsphericity. The orbits in this orientation space (θ, ϕ) may be visualized by plotting the trajectories on the unit sphere, as shown in Figure 5.4. The constant of integration, C, is known as the *orbital constant* and values in $0 \leq C < \infty$ determine orbits that range from the equator to a "degenerate orbit" consisting of a point at the "north pole." The exact shape of the orbit depends on the particle aspect ratio *via* the Bretherton constant B, as shown in Figure 5.5. For the sphere, we label a point on the surface to create artificially an axis of symmetry. For this situation, clearly the Jeffrey orbits correspond to lines of latitude; as the sphere spins about the z-axis with a constant angular velocity, the point label traces a cone. On the other hand, for slender bodies, $B \to 1$, the orbits approach great circles linking the positive and negative x-axes. The velocity along a given orbit now varies greatly. For example, at the orientation given by the point P_1, the slender body is swept out of alignment and reaches a maximum velocity at the point P_2. At point P_3, the orbital velocity is quite small, and the particle will spend most of the time in this orientation. However, as soon as the particle axis crosses the xz-plane, the cycle is repeated.

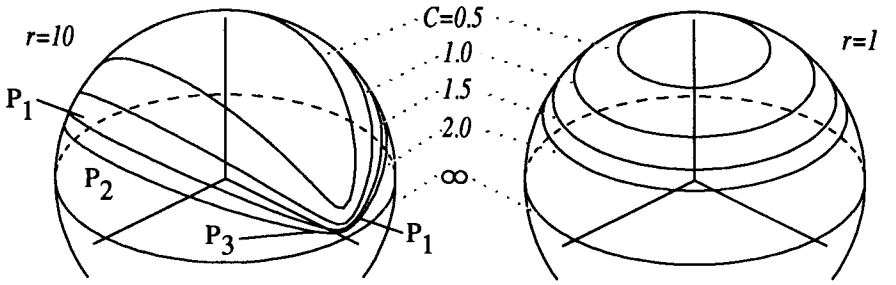

Figure 5.5: Jeffery orbits for different aspect ratios.

5.6 Rheology of a Dilute Suspension of Spheroids

The theoretical description of the rheological behavior of a dilute suspension of axisymmetric particles is one of the great "success stories" of microhydrodynamics. This endeavor has a long and distinguished history and the list of participants encompasses virtually all branches of the physical sciences, for this problem has served quite well as a model of the behavior (orientation *vs.* flow) of polymers in solutions. Our modest goal here is to illustrate how the resistance and mobility functions are used in the theoretical analysis; readers interested in a more complete physical picture are directed to the excellent reviews in in [7, 14]. A fairly complete review of the literature *circa* 1989 is available in Strand's doctoral dissertation [81].[6]

Jeffery [46] was the first to study the motion of a spheroid in a shear field, as a key step in an effort to extend Einstein's viscosity calculation to nonspherical (orientable) particles. After discovering this periodicity in the microhydrodynamics, he realized that a direct application of Einstein's idea would lead to a time periodic rheology. For instance, if a suspension of aligned prolate spheroids is sheared, the viscosity would undergo periodic oscillations, since the stresslet is smaller for a spheroid aligned in the direction of shear than for one transverse to the flow, $X^M < Y^M$. Real suspensions, on the other hand, exhibit fading memory, so that after several cycles these oscillations are damped out.

For a dilute suspension of submicron particles, rotary Brownian diffusion (Chapter 1) is the most plausible mechanism for the fading memory. With the inclusion of Brownian motion, the equations are no longer deterministic; rather, we describe the system as an ensemble with an orientation distribution function, $\psi(\boldsymbol{d}, t)$. The quantity $\psi(\boldsymbol{d}, t) \sin\theta \, d\theta \, d\phi$ gives the fraction of systems in the ensemble with particle orientations in the differential region about (θ, ϕ). The implications for the resulting rheological behavior of the suspension are now

[6]We acknowledge the assistance of Dr. Steven R. Strand in the preparation of this section.

clear. The ambient flow may orient the particle in certain preferred directions, but a nonuniform distribution of particle orientations leads to a "diffusive flux" from regions of high "concentration" to low "concentration."The resulting orientation distribution function determines the relative weighting of the stresslet functions in the particle contributions to the suspension stress. The balance between the flow-induced orientation and the randomizing influence of Brownian motion is affected by the flow strength, and thus the rheological property exhibits non-Newtonian behavior, such as shear thinning.

We start with the equation of continuity for ψ,

$$\frac{\partial \psi}{\partial t} + \nabla_d \cdot (\dot{\boldsymbol{d}}\psi) = 0 \ ,$$

and assign the following expression for $\dot{\boldsymbol{d}} = \omega \times \boldsymbol{d}$:

$$\dot{\boldsymbol{d}} = \boldsymbol{\omega} \times \boldsymbol{d} = \boldsymbol{\Omega}^{\infty} \times \boldsymbol{d} + \left(\frac{Y^H}{Y^C}\right)(\boldsymbol{E}^{\infty} \cdot \boldsymbol{d} - \boldsymbol{E}^{\infty} : \boldsymbol{ddd}) - (Y^C)^{-1} kT \frac{\partial}{\partial \boldsymbol{d}} \ln \psi \ .$$

Note that the effect of rotary Brownian motion comes in as a diffusive velocity. This equation may be obtained formally by starting with an angular momentum balance,

$$\boldsymbol{T}^{\mathrm{Hyd}} + \boldsymbol{T}^{\mathrm{Br}} = \boldsymbol{0} \ ,$$

with

$$\boldsymbol{T}^{\mathrm{Br}} = -\boldsymbol{d} \times \frac{\partial}{\partial \boldsymbol{d}}(kT \ln \psi) \ ,$$

and solving for ω.

The governing equation for ψ is thus a Fokker-Planck equation balancing Brownian diffusion and convection,

$$\frac{\partial \psi}{\partial t} + \left[\boldsymbol{\Omega}^{\infty} \times \boldsymbol{d} + \left(\frac{Y^H}{Y^C}\right)\boldsymbol{E}^{\infty} \cdot \boldsymbol{d}\right] \cdot \nabla_d \psi - 3\left(\frac{Y^H}{Y^C}\right)\boldsymbol{E}^{\infty} : \boldsymbol{dd}\,\psi = D_r \nabla_d^2 \psi \ , \quad (5.34)$$

with the rotary diffusion coefficent given by $D_r = kT/Y^C$.

For the shear flow problem and the parametrization of the particle axis in spherical polar coordinates, the diffusion equation becomes

$$\begin{aligned} \frac{1}{D_r}\frac{\partial \psi}{\partial t} &= -\frac{\dot{\gamma}}{D_r}\left[\frac{\sin\phi\cos\phi}{\sin\theta}\frac{\partial}{\partial\theta}(\psi \sin^2\theta\cos\theta) - \frac{\partial}{\partial\phi}(\psi\sin^2\phi)\right] \\ &+ \left[\frac{1}{\sin\theta}\frac{\partial}{\partial\theta}\left(\sin\theta\frac{\partial\psi}{\partial\theta}\right) + \frac{1}{\sin^2\theta}\frac{\partial^2\psi}{\partial\phi^2}\right] \ , \end{aligned} \quad (5.35)$$

where the second line is simply the angular parts of the Laplacian operator in spherical coordinates. The dimensionless group $P = \dot{\gamma}/D_r$ is often designated as a *Péclet* number, since it is a ratio of diffusive and convective time scales. Small P corresponds to fast diffusion over a weak flow, while large P corresponds to strong flows over weak diffusion.

We summarize a number of techniques for solving the orientation diffusion equation:

1. **Low Péclet Numbers.** When diffusion dominates over convection, we may solve for ψ using a regular perturbation in P. Without flow, the problem is quite simple and can be solved exactly. The next few terms in the small-P expansion for ψ are also obtained without too much difficulty [7, 31]. A procedure for generating these series on a computer is described in [49].

2. **High Péclet Numbers.** When strong convection dominates over weak diffusion, the problem may also be solved by a perturbation method, but a singular perturbation problem results, as expected by analogy with related problems in heat and mass transfer. Sharp gradients in ψ result near the slow regions of the Jeffrey orbits (the regions near the x-axis) and so, as shown in the work of Leal and Hinch [56], there are small "boundary layer" regions where diffusion is always important.

3. **Nearly Spherical Particles.** As mentioned above, the Jeffrey orbits take a particularly simple form for spheres. A perturbation solution in small deviations from sphericity is possible [67].

4. **Numerical Solutions (Galerkin Method).** The distribution function is expanded with the spatial dependence in terms of the spherical harmonics. The expansion is truncated at a finite number of terms, and the unknown coefficients are obtained by orthogonality conditions on the residual (the Galerkin method). Since the basis functions originate from the diffusion problem, although only a few terms are needed at small P, the number of terms in the expansion increases with P. However, with modest computational resources (minicomputers), this approach provides reliable solutions up to $P \sim 10^2$, thus bridging the gap between low and high Péclet number perturbation solutions. The Galerkin method was first applied to the orientation diffusion equation by Stewart and Sørensen [77] and the extension to the time-dependent equation is given in Strand *et al.* [82].

Given the orientation distribution, the bulk rheology is obtained by the ensemble average of the stresslet,

$$\begin{aligned} \boldsymbol{S} &= \boldsymbol{m} : \boldsymbol{E}^{\infty} - \boldsymbol{h} : \boldsymbol{T}^{\mathrm{Br}} \\ \sigma^{\mathrm{P}} &= < \boldsymbol{m} : \boldsymbol{E}^{\infty} > - < \boldsymbol{h} : \boldsymbol{T}^{\mathrm{Br}} > \ . \end{aligned}$$

The second term in the expression for the stresslet leads to the *direct Brownian contribution* to the bulk stress. (The *indirect* contribution is *via* the influence of Brownian motion on the orientation distribution and the resulting orientation averages). We may insert the resistance functions for the torque and stresslet on an axisymmetric particle to obtain the following expression relating the stress tensor with averages of moments of the particle orientation vector:

$$\sigma^{\mathrm{P}} = 2\mu c \{2A_H \boldsymbol{E}^{\infty} :< \boldsymbol{dddd} >$$

Hinch & Leal	Scheraga	Brenner
A	$J+K-L$	$(5/4)(3Q_2+4Q_3^0)$
B	$(L-M)/2$	$(5/2)Q_3^0$
C	M	$5Q_1$
F	N	$15N$

Hinch & Leal	Resistance functions
$8A$	$15X_1^M - 20Y_1^M + 5Z_1^M - 12B(r)Y_1^H$
$4B$	$5Y_1^M - 5Z_1^M + 3B(r)Y_1^H$
$2C$	$5Z_1^M$
F	$-9Y_1^H$

Table 5.1: The stress coefficients for steady shear flow.

$$+\ 2B_H(\boldsymbol{E}^\infty\cdot <\boldsymbol{dd}> + <\boldsymbol{dd}>\cdot\boldsymbol{E}^\infty - \frac{2}{3}\boldsymbol{\delta}\boldsymbol{E}^\infty :<\boldsymbol{dd}>$$
$$+\ C_H\boldsymbol{E}^\infty\ +\ F_HD_r(<\boldsymbol{dd}> -\frac{1}{3}\boldsymbol{\delta})\Big\}\ .$$

The notation follows Hinch and Leal [40] (which differs slightly from their later paper [41]), and the functions (A_H, B_H, C_H, F_H) are identical to their functions (A, B, C, F). The function D_r is the same rotary diffusivity that appears in the differential equation for the orientation distribution function. The relations to the standard resistance functions, as well as other notations found in the literature for the bulk stress, are given in Table 5.1.[7]

Figure 5.6 shows the behavior of the stress coefficients A_H, B_H, C_H, and F_H over a range of aspect ratios. The magnitude of all the functions becomes unbounded as the aspect ratio approaches zero. Functions A_H and F_H are also unbounded as r becomes large. Due to the complicated manner in which the stress coefficients A_H,B_H,C_H, and F_H depend on the spheroid aspect ratio, it is of interest to determine their limiting behavior for various important geometries: disk-like particles ($r \to 0$), nearly spherical particles ($r \to 1$), and rod-like particles ($r \to \infty$). The asymptotic forms are tabulated here and are in agreement with those of [40] except for the forms for C_H in the limits $r \to 1$ and $r \to 0$, which are in error in [40].

Hinch and Leal use the limiting values for the stress coefficients in developing expressions for the bulk stress for various limiting cases of particle shape

[7]Brenner [16], Hinch and Leal [40], and Kim [52] present expressions for the full stress tensor accounting for hydrodynamic and Brownian effects. Scheraga [72] presents an expression for the intrinsic viscosity; his notation is closely related to Jeffery's and has been widely cited.

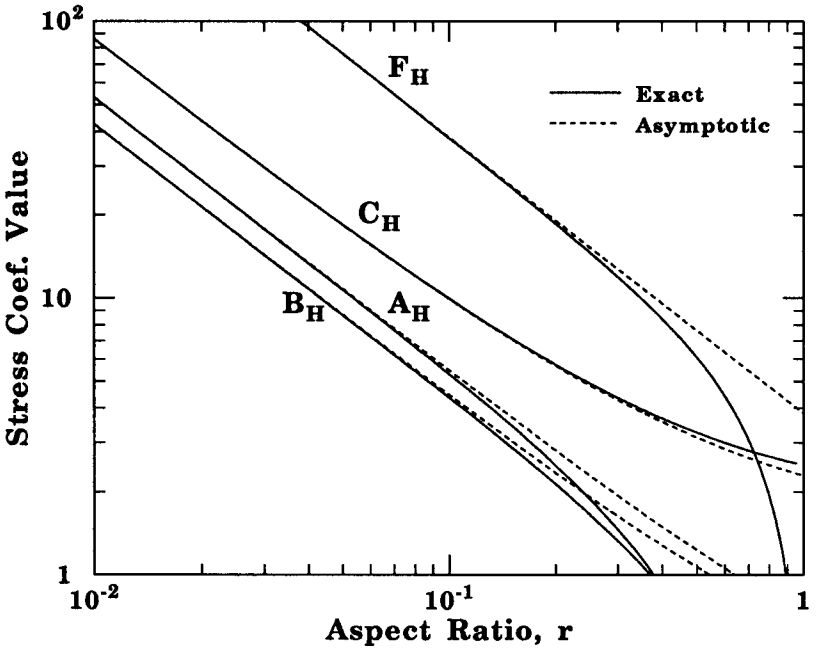

Figure 5.6: Comparison of asymptotic expressions with exact values of stress coefficients for oblate spheroids.

Coef.	$r \to \infty$	$\overset{r=1+\epsilon}{\epsilon \to 0}$	$r \to 0$
A_H	$\dfrac{r^2}{4(\ln(2r) - 3/2)}$	$\dfrac{395}{294}\epsilon^2$	$\dfrac{5}{3\pi r} + \left(\dfrac{104}{9\pi^2} - 1\right)$
B_H	$\dfrac{3\ln(2r) - 11/2}{r^2}$	$\dfrac{15}{28}\epsilon - \dfrac{895}{1176}\epsilon^2$	$\dfrac{-4}{3\pi r} + \left(\dfrac{1}{2} - \dfrac{64}{9\pi^2}\right)$
C_H	2	$\dfrac{5}{2} - \dfrac{5}{7}\epsilon + \dfrac{235}{294}\epsilon^2$	$\dfrac{8}{3\pi r} + \dfrac{128}{9\pi^2} + O(r^2)$
F_H	$\dfrac{3r^2}{\ln(2r) - 1/2}$	9ϵ	$-\dfrac{12}{\pi r} + O(r)$

Table 5.2: The limiting behavior of the stress coefficients.

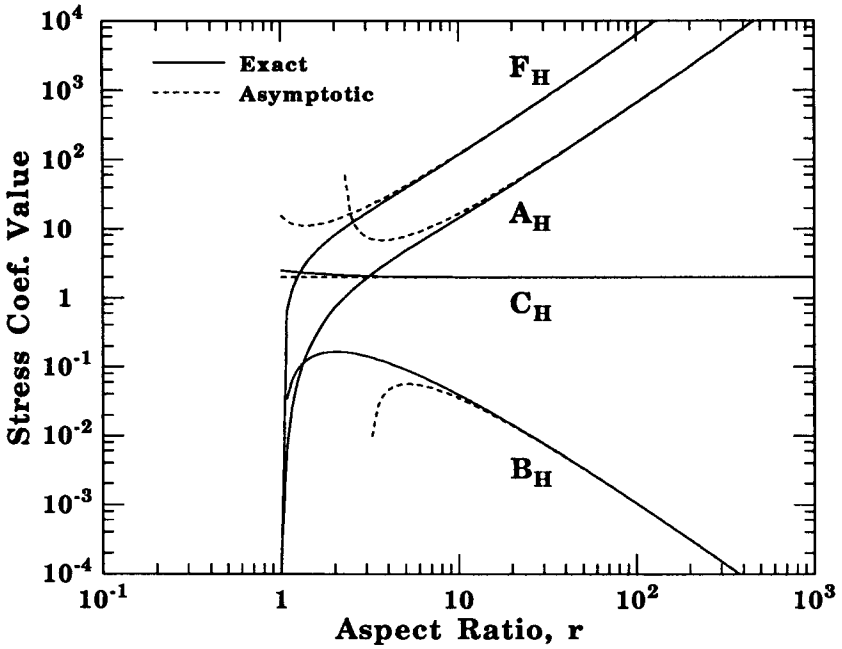

Figure 5.7: Comparison of asymptotic expressions with exact values of stress coefficients for prolate spheroids.

and shear strength. The range of validity of these asymptotic expressions is illustrated in the figures. The asymptotic expressions are quite close to the exact values over much of their individual ranges of interest, although it is apparent that the exact formulae are still needed for certain intermediate aspect ratios.

The intrinsic viscosity is an important material function for simple shear flow and is defined by

$$[\eta] = \lim_{c \to 0} \left(\frac{\sigma_{12} - \mu\dot{\gamma}}{c\mu\dot{\gamma}} \right) .$$

The results are plotted in the figure. As mentioned earlier, the balance between flow-induced orientation and Brownian motion results in non-Newtonian behavior. The viscosity exhibits shear-thinning; with increasing shear rate, a greater fraction of particles align with the flow and the particle contribution to the stress *via* the stresslet diminishes. The suspension also exhibits nonzero normal stress differences. For a review of these properties, as well as time-dependent rheological properties, we direct the reader to [7, 81] and references therein.

5.7 Electrophoresis

Electrophoresis, the motion of a charged particle under an applied electric field in an viscous electrolyte, is one of the most widely applied experimental methods

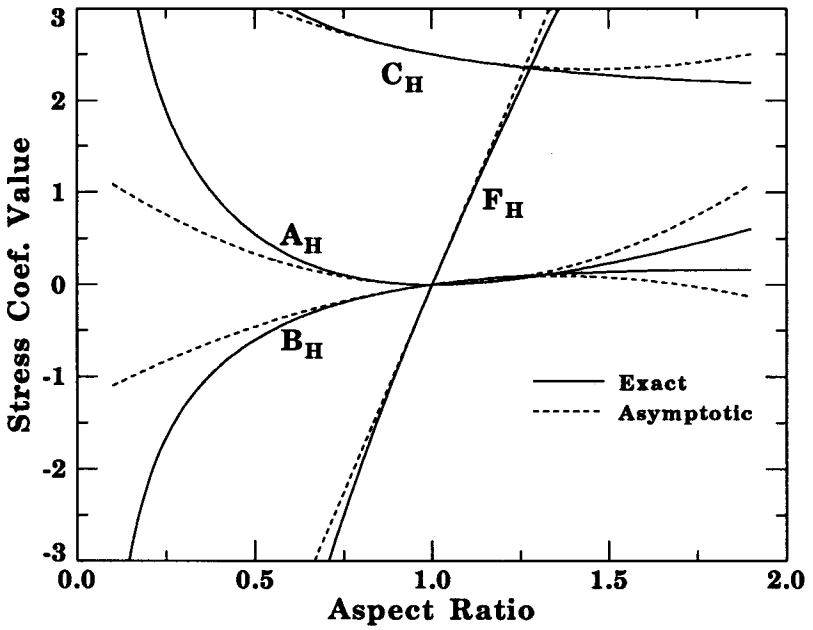

Figure 5.8: Comparison of asymptotic expressions with exact values of stress coefficients for spheroids of aspect ratio near unity.

in colloid research.[8] Separation and characterization of biochemical materials such as proteins by means of their electrophoretic properties are important operations in biochemistry and biophysics. In addition to such applications, electrophoresis is still used as a basic tool in studying the surface properties of colloidal substances.

The analysis of electrophoresis is essentially a study of the balance between the applied electrical force and the viscous resistance of the fluid. Indeed, for the so-called Hückel limit, the analysis is quite similar to that for sedimentation, in that the particle velocity follows from a balance of the external force (net charge on the particle $\times$ strength of the electric field) and the Stokes drag. If the counter-ions were not present (this is the limiting case of a very diffuse double layer), the electrophoretic velocity would be determined by equating the hydrodynamic drag force and the electrostatic force on the particle in an undisturbed applied field, as first proposed by Debye and Hückel [24, 43]. Thus for a spherical particle the electrophoretic mobility is given by

$$\frac{U}{E} = \frac{Q}{6\pi\mu a} = \frac{4\pi\epsilon\psi_0}{6\pi\mu a} = \frac{2\epsilon\psi_0}{3\mu} . \tag{5.36}$$

Here ψ_0 is the surface potential of the particle and ϵ is the permittivity of the

[8]We acknowledge the assistance of Dr. Byung J. Yoon in the preparation of this section.

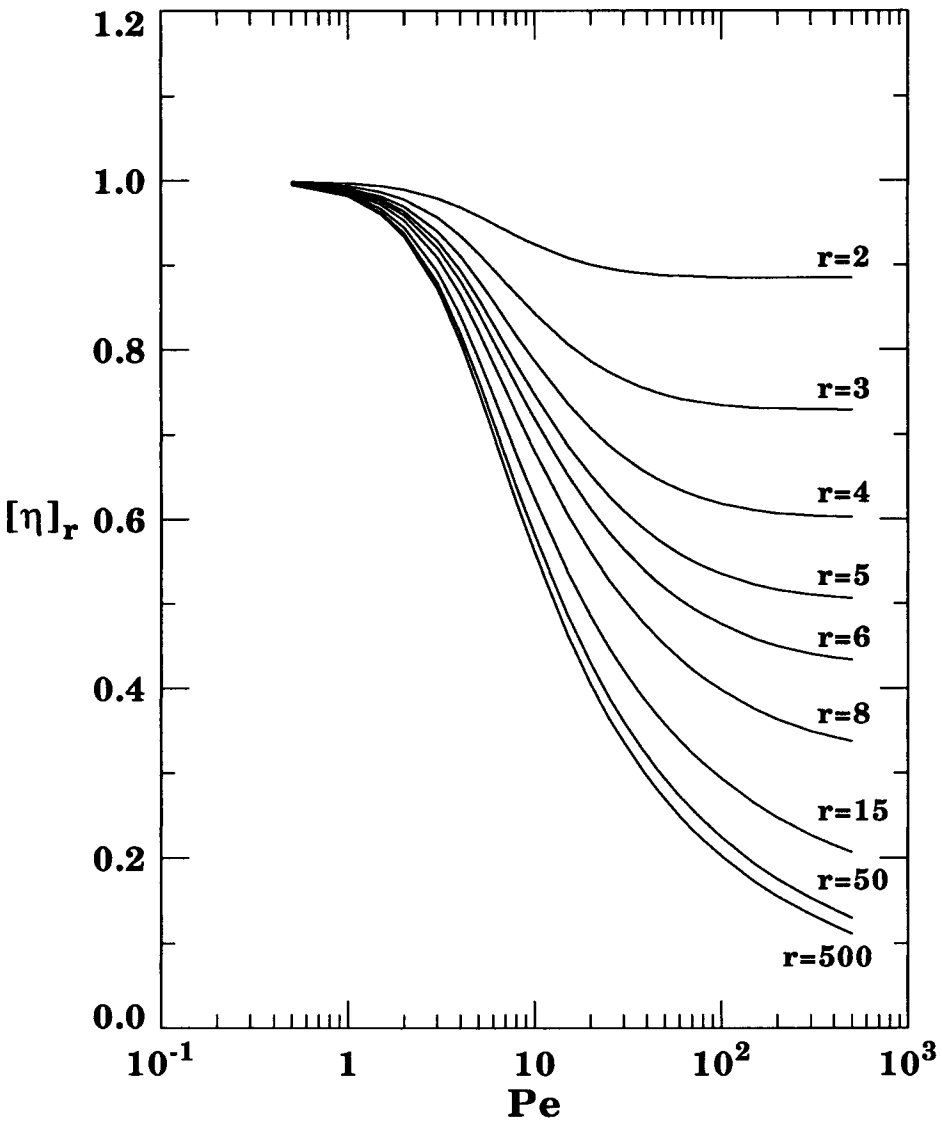

Figure 5.9: Intrinsic viscosity of a suspension of prolate spheroids in steady shear flow.

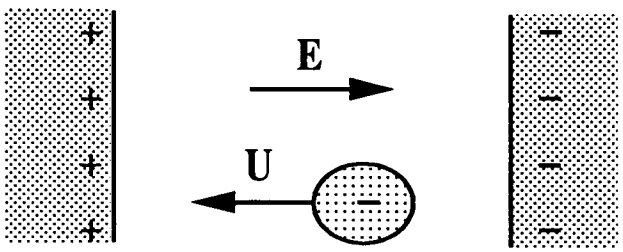

Figure 5.10: Electrophoresis of a charged particle in an electric field.

fluid.[9] The corresponding result for a spheroid using the appropriate resistance functions has also been noted [36].

For very thin double layers, or more precisely, when the radius of curvature of the particle surface is much larger than the double layer thickness, there is another simple limit known as the Helmholtz–Smoluchowski theory [76]. In this limit the electrophoretic velocity $\boldsymbol{U}$ of a rigid, nonconducting particle in an applied electric field $\boldsymbol{E}$ is given by

$$\frac{U}{E} = \frac{\epsilon\psi_0}{\mu} \,. \tag{5.37}$$

It is rather remarkable that Equation 5.37 holds for any particle shape if the above conditions plus a few more listed below are met. The proof is available in Morrison [62] and Teubner [85]. Essentially, the shape dependence of the viscous drag is canceled exactly by the same shape dependence of the electric force — this coming from the sheet of counter-ions fitting the particle form like a tight bodysuit. Later in this section we show that this is connected with the Lorentz reciprocal theorem and other machinery developed in this chapter. For situations of interest outside the two limiting regimes of very thin and very diffuse double layers, a more detailed analysis of the electroviscous forces is necessary.

The first critical analysis that takes into account the finite thickness of the double layer was reported by Henry [37]. Henry considered the electrophoretic motion of spherical particles and infinite cylinders aligned parallel or perpendicular to the electric field. He obtained the expressions for the electrophoretic

[9]The permittivity of a medium is defined by its appearance in Coulomb's law, $F = (Q_1Q_2)/4\pi\epsilon r^2$, where F is the force between point charges Q_1 and Q_2 separated by a distance r. The permittivity of a vacuum, denoted by ϵ_0, is $8.854 \times 10^{-12}\mathrm{kg}^{-1}\mathrm{m}^{-3}\mathrm{s}^4\mathrm{A}^2$. The dielectric constant of a material is the ratio between its permittivity and ϵ_0, and thus is a dimensionless quantity. Care should be exercised, since many authors (see, for example, the original papers by Debye and Hückel) prefer to use Gaussian units in which the unit of charge is defined so that $\epsilon_0 = 1$. For electrophoresis problems, the Gaussian result is readily obtained from ours by the formal operation: $\epsilon \to \epsilon/4\pi$. Jackson [45] contains a lucid description on units and dimensions of electrodynamics.

mobility as functions of the ratio between the particle radius and the thickness of the double layer, and showed that the Smoluchowski and the Hückel results were correct limits for spherical particles with a thin double layer and a thick double layer, respectively. In his analysis he assumed additivity of the imposed electric field in the presence of the particle and the field due to the equilibrium electric double layer. For the latter he used the solution of the linearized Poisson–Boltzmann equation (which we discuss shortly), which is valid only for small double layer potentials.

There are two major limitations in Henry's theory. Firstly, the deformation of the electric double layer around the particle during the electrophoretic motion is neglected. Since then many authors have treated this relaxation effect for spherical particles [8, 64, 91] and infinite cylinders [78, 79]. The relaxation effect gives a significant contribution when the thickness of the double layer is comparable to the particle radius and when the potentials are high. Secondly, only simple particle shapes, *i.e.*, spherical or cylindrical, are considered. Obviously, when the double layer is very thin, one can use the Smoluchowski equation, 5.37, irrespective of the particle shape. The thick double layer limit also can be easily determined for any particle geometry for which the resistance tensor is known. However, most colloidal particles are highly nonspherical, and the thickness of the double layer is comparable to the size of the particle in many cases.

5.7.1 Particles with Finite Electric Double Layers

In this subsection, we derive an expression for the electrophoretic mobility of nonspherical particles with double layers of finite thickness, following the exposition in Yoon [92]. We neglect the relaxation effect and assume small potentials around particles. We then discuss the special results obtained for sphere and spheroids, the latter being particularly important because many colloidal particles can be modelled as prolate spheroids (needle-like) or oblate spheroids.

A charged particle in an electrolyte (a solution of positive and negative ions), attracts a "cloud" of ions of opposite sign, also known as the counter-ions. In most colloidal systems, the particles are negatively charged, so the counter-ion cloud is composed of positive ions or cations. The charge distribution on the particle surface and in the counter-ion cloud together comprise the *diffuse double layer*, as shown in Figure 5.11. For a more complete discussion on the theory of colloidal phenomena, the diffuse electric double layer, and electrophoresis, we direct the reader to [25, 44, 75, 89].

Under equilibrium conditions, the ion concentrations follow the Boltzmann distribution,

$$n_\nu = n_\nu^\infty \exp(-z_\nu e\psi/kT) \,, \tag{5.38}$$

where z_ν is the valence of the ν-th ion species, n_ν^∞ is the ambient concentration far away from the particle, e is the fundamental charge, ψ is the electrosatic potential, k is the Boltzmann constant, and T is the absolute temperature. In other words, for each ion species, the distribution is influenced by the electric

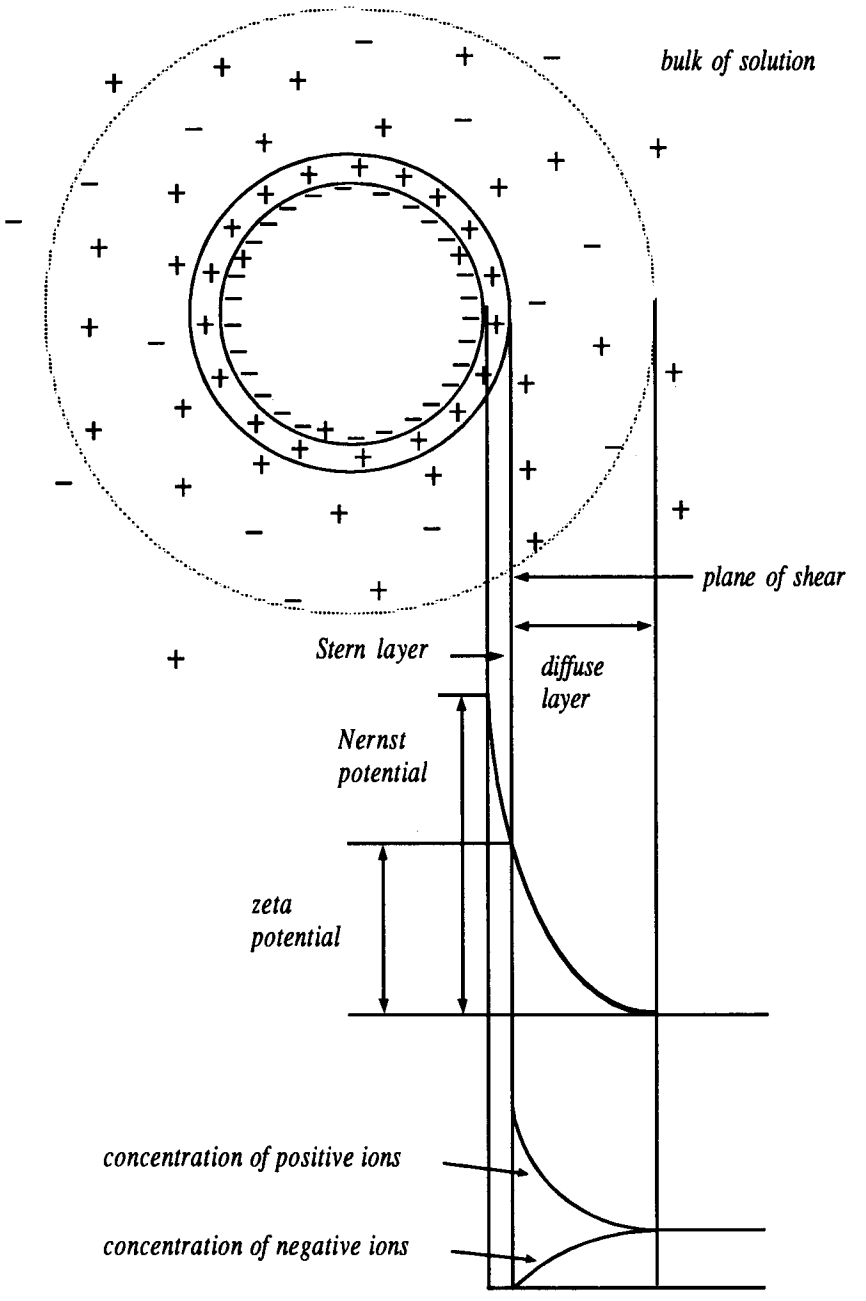

Figure 5.11: The diffuse double layer.

potential energy $z^\nu e\psi$, which pushes ions in the direction of lower potential energy, but Brownian diffusion of the ion, in the form of the thermal energy scale kT, imparts a diffusive flux that pushes the ions against the potential.

The charge distribution in the fluid, ρ_e, is obtained from these ionic concentrations as

$$\rho_e = e\sum_{\nu=1}^{n} n_\nu z_\nu \ . \tag{5.39}$$

Implicit in Equation 5.39 is the assumption that, on the length scale of interest, the ions in a differential volume element appear as a continuous charge distribution. Equations 5.38 and 5.39 dictate how the electrostatic potential influences the charge distribution, ρ_e. However, the charge distribution also determines the potential by Poisson's equation,

$$\nabla^2\psi = -\frac{\rho_e}{\epsilon} \ . \tag{5.40}$$

Combining Equations 5.39 and 5.40, we obtain the Poisson–Boltzmann equation,

$$\nabla^2\psi = -\frac{\rho_e(\psi)}{\epsilon} \ ,$$

which under condition of low potentials, $e\psi \ll kT$, reduces to the *linearized Poisson–Boltzmann equation*,

$$\nabla^2\psi - \kappa^2\psi = 0 \ , \tag{5.41}$$

with

$$\kappa^2 = \frac{e^2}{\epsilon kT}\sum_{\nu=1}^{n} n_\nu^\infty z_\nu^2 \ .$$

Here κ^{-1} has units of length and is known as the *Debye length.* It is the length scale associated with the exponential decay in the potential from the surface value to that of the ambient fluid. At distances much greater than κ^{-1}, the counter-ion cloud screens the charge on the particle and the potential decays exponentially to zero, in contrast to the inverse-separation decay of the Coulombic potential of a charged particle in a vacuum.

We now apply a uniform external electric field $\boldsymbol{E}$. When the applied field is small compared with the field due to the equilibrium double layer, we can assume additivity of the potentials. Neglecting the deformation of the double layer due to the applied field, we decompose the potential around the particle into two independent contributions: ψ from the equilibrium double layer and ϕ from the ambient field. The potential fields satisfy the equations

$$\begin{aligned} \nabla^2\psi &= \kappa^2\psi \ , \\ \nabla^2\phi &= 0 \ , \end{aligned}$$

with the boundary conditions

$$\begin{aligned} &\psi\,|_{r\to\infty} = 0 \ , \qquad \psi\,|_S = \psi_0 \ , \\ &\phi\,|_{r\to\infty} = -\boldsymbol{E}\cdot\boldsymbol{x} \ , \qquad \hat{\boldsymbol{n}}\cdot\nabla\phi\,|_S = 0 \ . \end{aligned}$$

We assume that the surface potential is constant and the dielectric constant of the particle is much smaller than that of the surrounding medium. But our results are not restricted to the situation with these boundary conditions, because the electrophoretic mobility is independent of the dielectric constant of the particle and the electrostatic boundary conditions on the particle surface [64].

The electric force on the particle has two distinct contributions. There is an electrostatic contribution given by

$$\int_{V_f} \rho_e \nabla\phi \, dV$$

and a hydrodynamic contribution due to the distribution of body forces $-\rho_e \nabla\phi$ throughout the fluid. Because of the Lorentz reciprocal theorem (see the discussion in Chapter 3 on the derivation of the Faxén law), this contribution is given exactly by

$$-\left[\int_{V_f} \tilde{u}_{ij} \rho_e \frac{\partial\phi}{\partial x_j} \, dV\right] ,$$

as first derived by Teubner [85]. The velocity field $\tilde{u}_{ij}$ represents the disturbance velocity field (j-th component) due to the translational motion of an uncharged particle (with a unit velocity along the i-axis). The hydrodynamic force is caused by the motion of the mobile ions in the diffuse double layer — in effect, the particle is moving not in a quiescent fluid, but against a local current of counter-ions flowing in the opposite direction under the action of the electric field. Since this hydrodynamic force acts against the motion of the particle, it is called the *electrophoretic retardation force.*

The force balance for the particle may be written as

$$\mu A_{ij} U_j = -\epsilon \left[\int_{V_f} \nabla^2\psi \frac{\partial\phi}{\partial x_i} \, dV\right] + \epsilon \left[\int_{V_f} \tilde{u}_{ij} \nabla^2\psi \frac{\partial\phi}{\partial x_j} \, dV\right] . \tag{5.42}$$

The left-hand side is the hydrodynamic force due to the motion of the particle and $\boldsymbol{A}$ is the resistance matrix for translation, discussed earlier in the chapter.

Using Green's second identity and the boundary condition on ϕ and ψ, we can rewrite the first volume integral into the surface integral over the particle surface S_p:

$$-\epsilon \left[\int_{V_f} \nabla^2\psi \frac{\partial\tilde{\phi}_k}{\partial x_i} \, dV\right] E_k \;=\; \epsilon \left[\oint_{S_p} \frac{\partial\psi}{\partial n} \frac{\partial\tilde{\phi}_k}{\partial x_i} \, dS\right] E_k \;=\; -\left[\oint_{S_p} \sigma \frac{\partial\tilde{\phi}_k}{\partial x_i} \, dS\right] E_k \, .$$

We now separate $\tilde{\phi}_k$ into two parts, one due to the ambient field, $-x_k$, and the second due to the disturbance field, denoted by $\tilde{\chi}_k$. The final result is

$$\mu A_{ij} U_j \;=\; \overbrace{\left[\int_{S_p} \sigma \, dS\right] E_i}^{\text{I}} + \overbrace{\left[\int_{S_p} -\sigma \frac{\partial\tilde{\chi}_k}{\partial x_i} dS\right] E_k}^{\text{II}} + \overbrace{\epsilon\left[\int_{V_f} -\tilde{u}_{ik} \nabla^2\psi \, dV\right] E_k}^{\text{III}}$$
$$+ \overbrace{\epsilon\left[\int_{V_f} \tilde{u}_{ij} \nabla\psi \frac{\partial\tilde{\chi}_k}{\partial x_j} \, dV\right] E_k}^{\text{IV}} \, . \tag{5.43}$$

Here I and II are the electrostatic forces on the surface charges due to the undisturbed applied electric field and the disturbance dipole electric field, respectively, while III and IV are the hydrodynamic drag forces on the particle due to the motion of the mobile ions. In III the ions move along the undisturbed applied field **E**, whereas in IV the ions move along the disturbance dipole field.

To solve the electrophoresis problem for an arbitrary particle under the assumptions of this section, we must first solve three boundary value problems: the linearized Poisson–Boltzmann equation to obtain ψ, the Laplace equation to get ϕ, and the Stokes equation for the translation of an uncharged particle through a quiescent fluid to get the velocity field $\tilde{u}_{ij}$. For the sphere, this is easily accomplished, and each integral in Equation 5.43 reduces to

$$\mathrm{I} = 4\pi\epsilon a\psi_0(1+\kappa a)\boldsymbol{E} \tag{5.44}$$

$$\mathrm{II} = \mathbf{0} \tag{5.45}$$

$$\mathrm{III} = -4\pi\epsilon a\psi_0\kappa a\boldsymbol{E} \tag{5.46}$$

$$\mathrm{IV} = 2\pi\epsilon a\psi_0\boldsymbol{E} + 12\pi\epsilon\int_a^\infty \psi\left[\left(\frac{a}{r}\right)^4 - \frac{5}{2}\left(\frac{a}{r}\right)^6\right] dr\,\boldsymbol{E}\,, \tag{5.47}$$

and summing these equations we recover[10] the result first obtained by Henry [37]:

$$\frac{U}{E} = \frac{\epsilon\psi_0}{\mu}\left[\frac{1}{6}(1+\kappa a) + \frac{1}{6}\left(12-(\kappa a)^2\right)\int_1^\infty \frac{e^{\kappa a(1-t)}}{t^5}\,dt\right]\,.$$

The ambient field contributions, I and III, are both linear to κa and have the same proportionality constants. Thus $O(\kappa a)$ terms cancel each other exactly and only the constant term $4\pi\epsilon a\psi_0\boldsymbol{E}$ survives. Obviously, this constant term corresponds to the Hückel limit.

The electrostatic force due to the disturbance field vanishes identically because of the isotropy of spherical particles. Since there is no effect of the double layer thickness on I + II + III, the hydrodynamic force in the disturbance dipole field is the only force that causes the transition from the Hückel limit to the Smoluchowski limit. This hydrodynamic force has the following asymptotic expressions:

$$\begin{aligned} \text{When } \kappa a \ll 1,\quad \mathrm{IV} &= 4\pi\epsilon a\psi_0\left(\frac{1}{16}\right)(\kappa a)^2\boldsymbol{E} \\ \text{When } \kappa a \gg 1,\quad \mathrm{IV} &= 2\pi\epsilon a\psi_0\boldsymbol{E} - 18\pi\epsilon a\psi_0\left(\frac{1}{\kappa a}\right)\boldsymbol{E}\,. \end{aligned} \tag{5.48}$$

It can be shown that this force is a monotonically increasing function of κa, and so the electrophoretic velocity of spheres increases with decreasing double layer thickness.

We note the following general points regarding Equation 5.43:

[10]The precise expression for the equivalent result in the original paper by Henry differs from ours, since his work is also in CGS units. As noted earlier, we may obtain his expressions by replacing our ϵ with $\epsilon/4\pi$.

1. A mobile ion moving perpendicular to the particle surface exerts more hydrodynamic force on the particle than one moving parallel to the particle surface. (This is the same reason why transverse flow around a prolate spheroid exerts more drag on the particle than an axisymmetric flow.) Thus the sign and magnitude of the hydrodynamic force (III or IV) is mainly determined by the amount of mobile ions moving perpendicular to the particle surface.

2. For nearly spherical particles the electrostatic force in a dipole field is almost zero because of its isotropic shape. But the hydrodynamic force in a dipole field has a finite value in consequence of (1). Since the dipole is oriented opposite to the applied field in the region where ions move perpendicular to the particle surface, this force is an enhancing one.

3. When the longest axis of spheroidal particles is aligned perpendicular to the applied field (Figure 5.12), one can easily see that the electrostatic force in a dipole field is a retarding one but the hydrodynamic force is an enhancing one. Since the magnitude of the hydrodynamic force is greater than that of the electrostatic force, the net force due to the dipole field is an enhancing one. When the longest axis of spheroidal particles is aligned parallel to the applied field (Figure 5.12), the signs of two forces are opposite to the perpendicular case and the electrostatic force is bigger than the hydrodynamic force. Thus the net force in a dipole field is again an enhancing one.

4. For particles with a thick double layer, the disturbance field contribution (II+IV) is negligible because the disturbance dipole field decays as r^{-3}. For particles with a thin double layer the domain that gives a significant contribution to the volume integrals is very small so that the contribution from the ambient field and the contribution from the disturbance field are of the same orders of magnitude. (Compare Equations 5.44 and 5.48, for example.)

5. When the double layer is very thick the electrophoretic motion of the particle is mainly determined by the balancing between the electrostatic force I (enhancing one) and the hydrodynamic force III (retarding one). The electrostatic force increases monotonically as κa increases and is independent of the particle orientation. The hydrodynamic force also increases monotonically, but does depend on the particle orientation. Thus the electrophoretic mobility of nonspherical particles may not be a monotonic function of κa in this region. This effect has been shown to occur for spheroids [92].

Although these arguments are based on Equation 5.43, where the deformation of the double layer is neglected, we can make the following qualitative observation on the electrophoretic motion of spherical particles with a deformed double layer. During the electrophoretic motion of the particle the total surface

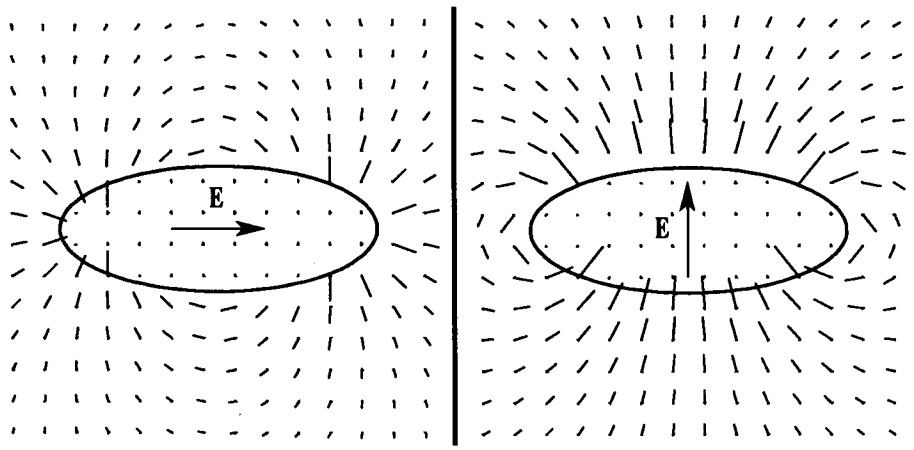

Figure 5.12: Alignment of spheroids in an applied electric field.

charge changes only slightly from the equilibrium (undeformed double layer) value, but the distribution of mobile ions in the diffuse double layer changes significantly. More counter-ions swarm behind the particle and move transversely. Thus, the hydrodynamic retardation force increases faster than the electrostatic force. Therefore, the electrophoretic velocity decreases for small κa. As κa increases the additional hydrodynamic force due to the disturbance field (enhancing one) becomes significant and the electrophoretic velocity increases accordingly.

The results for the electrophoretic mobility for oblate spheroids using Equation 5.43 are shown in Figure 5.13. For details of the calculation, we direct the reader to [92]. As noted above, the transition from the Hückel to the Smoluchowski limit is not monotonic.

5.7.2 Nonuniform Surface Potentials

We derive an expression for the electrophoretic velocity for a charged particle with nonuniform surface potential (also known as the zeta potential), assuming a thin electric double layer. The analysis follows the work of Fair and Anderson [27]. The fluid flow is driven by electrical stesses and the governing equations for the velocity and pressure are

$$\begin{aligned} -\nabla p + \mu \nabla^2 \boldsymbol{v} + \nabla \cdot \boldsymbol{m} &= \mathbf{0}\,, \qquad \nabla \cdot \boldsymbol{m} = \rho_e \boldsymbol{E}\,, \\ \nabla \cdot \boldsymbol{v} &= \mathbf{0} \\ \text{on } S_p \quad \boldsymbol{v} &= \boldsymbol{U} + \boldsymbol{\omega} \times \boldsymbol{x}\,. \end{aligned}$$

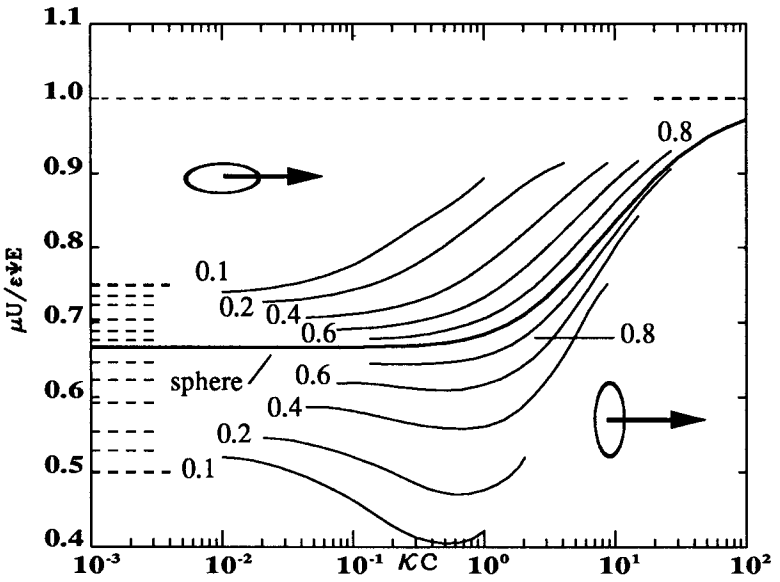

Figure 5.13: Electrophoretic mobility of oblate spheroids.

The electrical stress $\boldsymbol{m}$ is also known as the Maxwell stress. We assume a thin double layer everywhere so that $\kappa \bar{R} \gg 1$, *i.e.*, everywhere the local radius of curvature $\bar{R}$ is much greater than the double layer thickness. We may use the method of matched asymptotic expansions. To leading order, in the inner region $y \sim O(\kappa^{-1})$, where y is the normal coordinate for the local plane geometry near the surface. The governing equations reduce to

$$\begin{aligned} \mu \frac{\partial^2 \boldsymbol{v}}{\partial y^2} &= -\rho_e \boldsymbol{E}_s \\ \rho_e &= -\epsilon \frac{\partial^2}{\partial y^2}(\phi - \phi_s) \\ \text{on } S_p \quad \boldsymbol{v} &= \boldsymbol{U} + \boldsymbol{\omega} \times \boldsymbol{x} \ , \end{aligned}$$

where $\phi_s = \lim_{\kappa y \to \infty} \phi$ and $\boldsymbol{E}_s = -\nabla \phi_s$. The velocity profile may be integrated over the double layer region to give the matching condition,

$$\text{on } S_p^+ \quad \boldsymbol{v} = \boldsymbol{U} + \boldsymbol{\omega} \times \boldsymbol{x} + \boldsymbol{v}^{(S)} \ , \qquad \boldsymbol{v}^{(S)} = -\frac{\epsilon}{\mu} \psi_0 \boldsymbol{E}_s \ . \tag{5.49}$$

Outside the double layer ρ_e is negligible so the electrical stresses vanish. The governing equations in the outer region are thus the Stokes equations, with the modified boundary condition, Equation 5.49. Since $\nabla \cdot (\boldsymbol{\sigma} + \boldsymbol{m}) = \boldsymbol{0}$ in the outer fluid, we find that the net force and torque is zero on S_p^+.

Even though we apply the usual no-slip boundary condition for $\boldsymbol{v}$, the outer problem sees an apparent *Smoluchowski slip velocity* $\boldsymbol{v}^{(S)}$, but not the sharp

gradient inside the double layer. Using the linearity of the Stokes equations, we may write the force and torque on S_p^+ as the sum of contributions due to the rigid-body motion and that due to the slip velocity

$$\boldsymbol{F} = \oint_{S_p^+} \sigma \cdot \hat{\boldsymbol{n}} \;=\; -\mu \boldsymbol{A} \cdot \boldsymbol{U} - \tilde{\boldsymbol{B}} \cdot \boldsymbol{\omega} + \boldsymbol{F}^{(S)} = \boldsymbol{0} \;, \tag{5.50}$$

$$\boldsymbol{T} = \oint_{S_p^+} \boldsymbol{x} \times \sigma \cdot \hat{\boldsymbol{n}} \;=\; -\mu \boldsymbol{B} \cdot \boldsymbol{U} - \boldsymbol{C} \cdot \boldsymbol{\omega} + \boldsymbol{T}^{(S)} = \boldsymbol{0} \;. \tag{5.51}$$

The contributions from the slip velocity may be cast in an alternate form using the Lorentz reciprocal theorem, *e.g.*,

$$\boldsymbol{F}^{(S)} = \oint_{S_p^+} \boldsymbol{\delta} \cdot \boldsymbol{\sigma}^{(S)} \cdot \hat{\boldsymbol{n}} \, dS = \oint_{S_p^+} \boldsymbol{v}^{(S)} \cdot \boldsymbol{\sigma}(;\boldsymbol{\delta}) \cdot \hat{\boldsymbol{n}} \, dS \;,$$

where $\boldsymbol{U} \cdot \boldsymbol{\sigma}(;\boldsymbol{\delta}) \cdot \hat{\boldsymbol{n}}$ is the surface traction generated by the particle translating with velocity $\boldsymbol{U}$. After substitution of the expresson for the slip velocity, we obtain the result,

$$\mu \boldsymbol{A} \cdot \boldsymbol{U} + \tilde{\boldsymbol{B}} \cdot \boldsymbol{\omega} \;=\; -\frac{\epsilon}{\mu} \oint_{S_p^+} \psi_0 \boldsymbol{\sigma}(;\boldsymbol{\delta}) \cdot \hat{\boldsymbol{n}} \, dS \cdot \boldsymbol{E}_s \tag{5.52}$$

$$\mu \boldsymbol{B} \cdot \boldsymbol{U} + \boldsymbol{C} \cdot \boldsymbol{\omega} \;=\; -\frac{\epsilon}{\mu} \oint_{S_p^+} \psi_0 \boldsymbol{\sigma}(;\boldsymbol{\delta} \times \boldsymbol{x}) \cdot \hat{\boldsymbol{n}} \, dS \cdot \boldsymbol{E}_s \;, \tag{5.53}$$

which may be inverted using the mobility functions $\boldsymbol{a}$, $\boldsymbol{b}$, and $\boldsymbol{c}$ to yield explicit expressions for the particle motion. Equations 5.52 and 5.53 are especially applicable in situations in which the potential varies along the surface of the particle.

If the particle is at a constant potential, we may move ψ_0 out of the integral. The surface integrations of the RBM-tractions then yield the resistance functions $\boldsymbol{A}$ and $\boldsymbol{C}$. *For a particle with* $\boldsymbol{B} = \boldsymbol{0}$, *the shape dependence disappears from the electrophoretic mobility* and we obtain the vector form of Smoluchowski's celebrated result (Equation 5.37). This idea is readily generalized to show that an assembly of particles at constant zeta potential and thin double layer all move with the same Smoluchowski velocity [48]. This can lead to quite dramatic effects. Since hydrodynamic interactions are essentially zero for this situation, theories developed for dilute suspensions still apply at very high concentrations as shown in [93].

Exercises

Exercise 5.1 Symmetry Relations for the Resistance and Mobility Functions.

Derive all of the symmetry relations for the resistance and mobility functions [39].

Hint: The selection of $\boldsymbol{v}_1$ and $\boldsymbol{v}_2$ should be motivated by the resistance and mobility tensors of interest.

Exercise 5.2 The Hydrodynamic Center is Well Defined.
Show that result for the hydrodynamic center, Equation 5.11, is independent of the choice of the reference point, $\boldsymbol{x}_1$.

Exercise 5.3 The Hydrodynamic Center of a Dumbbell.
Consider a dumbbell formed by two unequal spheres joined by a rigid rod of negligible friction. Use Equation 5.11 to show that, neglecting hydrodynamic interactions between the spheres, the hydrodynamic center is at

$$\boldsymbol{x}_{cr} = \frac{a_1 \boldsymbol{x}_1}{a_1 + a_2} + \frac{a_2 \boldsymbol{x}_2}{a_1 + a_2} .$$

In other words, the hydrodynamic center lies on the dumbbell axis with the distance from the sphere centers weighted by sphere radii.

Exercise 5.4 The Hydrodynamic Center of a Propeller.
Consider the propeller-shaped body of Figure 5.1. Use symmetry to show that there exists a point on the axis where the three principal directions satisfy $\boldsymbol{B}(\boldsymbol{0}) \cdot \boldsymbol{e}_1 = \boldsymbol{0}$, $\boldsymbol{B}(\boldsymbol{0}) \cdot \boldsymbol{e}_2 \parallel \boldsymbol{e}_2$, and $\boldsymbol{B}(\boldsymbol{0}) \cdot \boldsymbol{e}_3 \parallel \boldsymbol{e}_3$, where $\boldsymbol{e}_1$ is directed along the axis of one of the blades.

From Equation 5.11 for the hydrodynamic center, we conclude that this point is the hydrodynamic center.

Exercise 5.5 Bounds for an Axisymmetric Body in a Linear Field.
Consider a force-free axisymmetric particle in a two-dimensional linear flow field confined to the xy-plane, *i.e.*, $\boldsymbol{v}^\infty = \boldsymbol{\kappa} \cdot \boldsymbol{x}$ with

$$\boldsymbol{\kappa} = \begin{pmatrix} \kappa_{11} & \kappa_{12} & 0 \\ \kappa_{21} & \kappa_{22} & 0 \\ 0 & 0 & 0 \end{pmatrix} .$$

Show that at the instant that the particle is oriented along the y-axis, the torque and stresslet in this ambient field require only the resistance functions Y^C, Y^H, and Y^M. Then use energy dissipation arguments to derive an inequality of the form

$$(Y^H)^2 < \alpha Y^C Y^M , \qquad \text{or} \qquad \left(\frac{Y^H}{Y^C}\right)^2 < \alpha \frac{Y^M}{Y^C} .$$

Find the value of α. Note that the last expression gives an upper bound for the Bretherton constant.

Exercise 5.6 Inclusion Monotonicity for the Resistance Tensor.
In this exercise, we derive the inclusion monotonicity for the resistance tensor. Let $\mathcal{R}$ and $\mathcal{R}'$ denote the resistance matrices of two particles, with the primed particle completely inside the other. Denote the "vector" formed by concatenation of $\boldsymbol{U}^\infty - \boldsymbol{U}$, $\boldsymbol{\Omega}^\infty - \boldsymbol{\omega}$, and $\boldsymbol{E}^\infty$ by $\mathcal{U}$. Show that the inclusion monotonicity of Chapter 2 may be expressed as a statement concerning the resistance matrices, that for all $\mathcal{U}$,

$$0 < \mathcal{U} \cdot \mathcal{R}' \cdot \mathcal{U} \leq \mathcal{U} \cdot \mathcal{R} \cdot \mathcal{U} .$$

Exercise 5.7 Inclusion Monotonicity for the Mobility Tensor.
In this exercise, we derive the inclusion monotonicity for the mobility tensor. Let $\mathcal{M}$ and $\mathcal{M}'$ denote the mobility matrices of two particles, with the primed particle completely inside the other. Denote the "vector" formed by concatenation of $\boldsymbol{F}$ and $\boldsymbol{T}$ by $\mathcal{F}$. Show that the inclusion monotonicity of Chapter 2 may be expressed as a statement concerning the mobility matrices, that for all $\mathcal{F}$,

$$0 < \mathcal{F} \cdot \mathcal{M} \cdot \mathcal{F} \leq \mathcal{F} \cdot \mathcal{M}' \cdot \mathcal{F} \ .$$

Does this result follow directly from Exercise 3.7? If A and B are two positive-definite matrices, does $A < B$ imply $A^{-1} > B^{-1}$? Here, the ordering $A < B$ is defined by the difference $B - A$ being positive-definite.
Hint: Use the properties of positive-definite matrices, in particular the existence of $A^{-1/2}$ (see [30, 83]).

Exercise 5.8 Electrophoresis: Thick Electric Double Layers.
Show that in the limit of a thick electric double layer, $\kappa a \to 0$, Equation 5.43 reduces to the Hückel limit for the electrophoretic velocity,

$$\boldsymbol{U} = \frac{Q}{\mu} \boldsymbol{A}^{-1} \cdot \boldsymbol{E} \ .$$

Exercise 5.9 Electrophoresis: Thin Electric Double Layers.
Show that in the limit of a thin electric double layer, $\kappa a \to \infty$, Equation 5.43 reduces to the Smoluchowski limit for the electrophoretic mobility,

$$\boldsymbol{U} = \frac{\epsilon}{\mu} \psi_0 \boldsymbol{E} \ ,$$

so that the electrophoretic mobility is independent of particle size and shape.

Exercise 5.10 Electrophoresis of Spheres at Nonuniform Surface Potentials.
Show that for a sphere, Equation 5.52 simplifies to

$$\boldsymbol{U} = \frac{\epsilon}{\mu} \bar{\psi}_0 \boldsymbol{E}_s \ ,$$

where $\bar{\psi}_0$ is the area-averaged surface potential on the sphere.

Exercise 5.11 Electrophoresis of a Prolate Spheroid at Nonuniform Surface Potentials.
Consider a surface potential of the form

$$\psi_0 = \beta_0 + \beta_2 z^2 \ .$$

Show that by interpreting $\psi_0 \boldsymbol{E}_s$ as an ambient velocity field for the effective Stokes flow problem, the tedious algebra involved with the direct use of Equation 5.52 may be bypassed by the use of the Faxén law for the prolate spheroid. Show that it is possible for a prolate spheroid with zero net charge to undergo electrophoresis.